NAC-0015_R1

Unsaturated Zone Modeling for the Clive PA

Clive DU PA Model v1.2

12 June 2014

Prepared for Energy*Solutions* by
NEPTUNE AND COMPANY, INC.
1505 15th St, Suite B, Los Alamos, NM 87544

1. Title: Unsaturated Zone Modeling for the Clive PA		
2. Filename: Unsaturated Zone Modeling V2.docx		
3. Description: This white paper provides documentation of the development of parameter values and distributions used for modeling liquid phase transport in the saturated zone for the Clive DU PA model.		
	Name	Date
4. Originator	Michael Sully	5 May 2014
5. Reviewer	Dan Levitt	21 May 2014

6. Remarks

5/8/2014: DL. Added new section 14.0 that discusses nine H1D sensitivity runs that evaluate effects of Rn barrier Ksat and rooting depth on infiltration.

5/9/2014: MS. The element names in GoldSim for α and n were changed. Element names were revised in white paper.

5/13/2014: MS. Revised distribution for van Genuchten alpha and n from using standard deviations to standard errors.

5/13/2014: DL. Added text justifying use of 1D model.

5/17/2014: MS: Expanded discussion of 2D vs 1D.

6/8/2014: MS: Added reference to method described in Appendix for estimating water content for waste, clay liner, and unsaturated zone.

6/11/2014: MS Added Runge-Kutta method Appendix to pdf.

CONTENTS

FIGURES

TABLES

1.0 Summary of Parameter Values and Distributions

A summary of parameter values used in the Clive DU PA Model is provided in Table 1. For distributions, the following notation is used:

- N(μ, σ, [*min*, *max*]) represents a normal distribution with mean μ and standard deviation σ, and optional truncation at the specified *min*imum and *max*imum,
- LN(*GM*, *GSD*, [*min*, *max*]) represents a log-normal distribution with geometric mean GM and geometric standard deviation GSD, and optional *min* and *max*,
- U(*min*, *max*) represents a uniform distribution with lower bound *min* and upper bound *max*,
- Beta(μ, σ, *min*, *max*) represents a generalized beta distribution with mean μ, standard deviation σ, minimum *min*, and maximum *max*,
- Gamma(μ, σ) represents a gamma distribution with mean μ and standard deviation σ, and
- TRI(*min*, *m*, *max*) represents a triangular distribution with lower bound *min*, mode *m*, and upper bound *max*.

Note that a number of these distributions are truncated at a minimum value of 0 and a maximum of Large, an arbitrarily large value defined in the GoldSim model. The truncation at the low end is a matter of physical limits (e.g. precipitation cannot be negative), and in GoldSim's distribution definitions, if truncations are made, they must be made at both ends, so the very large value is chosen for the upper end.

Table 1. Summary of Parameter Values and Distributions

Parameter	Distribution [*Comments*]	Units	Internal Reference
Infiltration and Water Content			
VG_logAlpha	N(μ=-1.79, σ=0.1209, (min=-Large, max=0)	$\log_{10}$(1/cm)	Section 12.5
VG_logN	N(μ=0.121, σ=0.0189, (min=Small, max=Large);	—	Section 12.5
RnBarrierKsat_Natdist	LN(0.691, 6.396); [*right shift of 0.00432*]	cm/day	Section 12.5
WaterContentResidual			
SurfaceSoil	0.11	—	Section 12.5, Table 8
EvapLayer	0.11	—	Section 12.5, Table 8
FrostLayer	0.065	—	Section 12.5, Table 8
UpperRnBarrier	0.1	—	Section 12.5, Table 8
LowerRnBarrier	0.1	—	Section 12.5, Table 8

Parameter	Distribution [*Comments*]	Units	Internal Reference
Cover Layers Infiltration and Water Content Regression Parameters			
Response Variable	**β_0**		
Infiltration flux (through all layers)	0.959	—	Section 12.9
Water content in Surface Layer	0.554	—	Section 12.9
Water content in Evaporative zone layer	0.684	—	Section 12.9
Water content in Frost Protection layer	0.0726	—	Section 12.9
Water in Upper Radon Barrier	0.03	—	Section 12.9
Water in Lower Radon Barrier	0.03	—	Section 12.9
Response Variable	**β_1**		
Infiltration flux (through all layers)	0.0	—	Section 12.9
Water content in Surface Layer	-0.00197	—	Section 12.9
Water content in Evaporative zone layer	-0.00222	—	Section 12.9
Water content in Frost Protection layer	-0.000169	—	Section 12.9
Water in Upper Radon Barrier	-0.00361	—	Section 12.9
Water in Lower Radon Barrier	-0.00361	—	Section 12.9
Response Variable	**β_2**		
Infiltration flux (through all layers)	4.4	—	Section 12.9
Water content in Surface Layer	-0.0555	—	Section 12.9
Water content in Evaporative zone layer	-0.157	—	Section 12.9
Water content in Frost Protection layer	0.0521	—	Section 12.9
Water in Upper Radon Barrier	0.314	—	Section 12.9
Water in Lower Radon Barrier	0.314	—	Section 12.9
Response Variable	**β_3**		
Infiltration flux (through all layers)	-0.521	—	Section 12.9
Water content in Surface Layer	-0.222	—	Section 12.9
Water content in Evaporative zone layer	-0.288	—	Section 12.9
Water content in Frost Protection layer	-7.27×10^{-6}	—	Section 12.9
Water in Upper Radon Barrier	-0.013	—	Section 12.9
Water in Lower Radon Barrier	-0.013	—	Section 12.9
Fate and Transport			
Water tortuosity water content exponent	N(μ=7/3, σ=0.01)	—	Section 15.1.3
Water tortuosity porosity exponent	N(μ=2.0, σ=0.01	—	Section 15.1.3

Parameter	Distribution [*Comments*]	Units	Internal Reference
Thickness of the atmosphere layer	N(μ=2.0, σ=0.5, min=Small, max=Large)	M	Section 15.2.2, Table 12
Wind speed	N(μ=3.14, σ=0.5, min=Small, max=Large)	m/s	Section 15.2.2, Table 12
Atmospheric diffusion length	N(μ=0.1, σ=0.02, min=Small, max=Large)	m	Section 15.2.2, Table 12
Thickness of the Unsat zone (below the embankment clay liner)	N(12.9, 0.25, min=small, max=Large)	ft	Section 11
Unit 3			
Porosity_Unit3	equal to MCsat_Unit3	—	Section 7.3
BulkDensity_Unit3	N(ParticleDensity_Unit3 × (1 – Porosity_Unit3), 0.1, min=Small, max=Large)	g/cm^3	Section 7.3
ParticleDensity_Unit3	2.65	g/cm^3	Section 7.3
D_Unit3	N(2.73, 5.21e-3, min=0, max=3)	—	Section 7.4.1
Hb_Unit3	N(8.85, 0.929, min=Small, max=Large); [*correlated to D_Unit3 as -0.85*]	cm	Section 7.4.1
MCres_Unit3	N(6.78e-3, 2.05e-3, min=Small, max=Large); [*truncated just above 0*]	—	Section 7.4.1
MCsat_Unit3	N(0.393, 6.11e-3, min=Small, max=1-Small), [*truncated just above 0 and just below 1*]	—	Section 7.4.1
Ksat_Unit3	N(5.14e-5, 5.95e-6, min=Small, max=Large); [*correlated to D_Unit3 as -0.98*]	cm/s	Section 7.4.1
Unit 4			
Porosity_Unit4	equal to MCsat_Unit4	—	Section 7.3
BulkDensity_Unit4	N(ParticleDensity_Unit4 × (1 – Porosity_Unit4), 0.1, min=Small, max=Large); [*truncated just above 0*]	g/cm^3	Section 7.3
ParticleDensity_Unit4	2.65	g/cm^3	Section 7.3

Parameter	Distribution [*Comments*]	Units	Internal Reference
D_Unit4	N(2.81, 9.93e-5, min=0, max=3)	—	Section 7.4.2
Hb_Unit4	N(104., 1.72, min=Small, max=Large); [*correlated to D_Unit4 as -0.66*]	cm	Section 7.4.2
MCres_Unit4	N(0.108, 8.95e-4, min=Small, max=Large); [*truncated just above 0*]	—	Section 7.4.2
MCsat_Unit4	N(0.428, 6.08e-3, min=Small, max=1-Small); [*truncated just above 0 and just below 1*]	—	Section 7.4.2
Ksat_Unit4	N(5.16e-5, 5.97e-7, min=Small, max=Large); [*truncated just above 0; correlated to D_Unit4 as -0.37*]	cm/s	Section 7.4.2
Upper Radon Barrier Clay			
Porosity_UpperRnBarrierClay	assigned value for Unit 4	—	Section 7.3
BulkDensity_UpperRnBarrierClay	assigned value for Unit 4	g/cm^3	Section 7.3
Lower Radon Barrier Clay			
Porosity_LowerRnBarrierClay	assigned value for Unit 4	—	Section 7.3
BulkDensity_LowerRnBarrierClay	assigned value for Unit 4	g/cm^3	Section 7.3
Generic Waste			
Porosity_Generic_Waste	assigned value for Unit 3	—	Section 7.3
BulkDensity__Generic_Waste	assigned value for Unit 3	g/cm^3	Section 7.3
D_Generic_Waste	assigned value for Unit 3	—	Section 7.4.1
Hb_Generic_Waste	assigned value for Unit 3	cm	Section 7.4.1
MCres_Generic_Waste	assigned value for Unit 3	—	Section 7.4.1
MCsat_Generic_Waste	assigned value for Unit 3	—	Section 7.4.1
Ksat_Generic_Waste	assigned value for Unit 3	cm/s	Section 7.4.1
UO3 Waste			
Porosity_Generic_Waste	assigned value for Unit 3	—	Section 7.3
BulkDensity__Generic_Waste	assigned value for Unit 3	g/cm^3	Section 7.3
D_Generic_Waste	assigned value for Unit 3	—	Section 7.4.1
Hb_Generic_Waste	assigned value for Unit 3	cm	Section 7.4.1

Parameter	Distribution [*Comments*]	Units	Internal Reference
MCres_Generic_Waste	assigned value for Unit 3	—	Section 7.4.1
MCsat_Generic_Waste	assigned value for Unit 3	—	Section 7.4.1
Ksat_Generic_Waste	assigned value for Unit 3	cm/s	Section 7.4.1
U3O8 Waste			
Porosity_Generic_Waste	assigned value for Unit 3	—	Section 7.3
BulkDensity__Generic_Waste	assigned value for Unit 3	g/cm^3	Section 7.3
D_Generic_Waste	assigned value for Unit 3	—	Section 7.4.1
Hb_Generic_Waste	assigned value for Unit 3	cm	Section 7.4.1
MCres_Generic_Waste	assigned value for Unit 3	—	Section 7.4.1
MCsat_Generic_Waste	assigned value for Unit 3	—	Section 7.4.1
Ksat_Generic_Waste	assigned value for Unit 3	cm/s	Section 7.4.1
Liner Clay			
Porosity_LinerClay	assigned value for Unit 4	—	Section 7.3
BulkDensity__LinerClay	assigned value for Unit 4	g/cm^3	Section 7.3
D_LinerClay	assigned value for Unit 4	—	Section 7.4.2
Hb_LinerClay	assigned value for Unit 4	cm	Section 7.4.2
MCres_LinerClay	assigned value for Unit 4	—	Section 7.4.2
MCsat_LinerClay	assigned value for Unit 4	—	Section 7.4.2
Ksat_LinerClay	LN(1e-6, 1.2)	cm/s	Section 7.4.2

Porous medium solid/water partition coefficients for various radionuclides in these materials are assigned one of three representative and rather generic collections of K_d values for the materials sand, silt and clay. These assignments are listed in Table 2, with discussion in the relevant sections below. Distributions for the values themselves are documented in the *Geochemical Modeling* white paper.

Table 2. Assignment of solid/water partition coefficients K_d values.

material	*K_d material*
Unit 2 (includes saturated zone medium)	clay
Unit 3 (includes unsaturated zone medium and all wastes)	sand
Unit 4 (includes surface layer, evaporative zone, clay liner, and upper and lower radon barrier clays)	silt

2.0 Introduction

This white paper provides documentation of the development of parameter values and distributions used for modeling gas and liquid phase transport in the unsaturated zone for the Clive DU PA model. Data sources are identified and the rationale applied in developing distributions is described. The intent of this white paper is to describe the characteristics and processes in the disposal cell, waste and the underlying unsaturated zone above the shallow aquifer. Estimates of net infiltration through the evapotranspiration (ET) cover system layers and material water content required by the GoldSim model (the DU PA Model) were made using the HYDRUS-1D software package (Šimůnek et al., 2009) and are described in this white paper. Saturated zone characteristics and processes are described in the Saturated Zone Modeling white paper.

3.0 Disposal Cell Design

Engineered barriers are used at the Clive site to control the flow of water into the waste. The portion of Federal Cell housing DU (the Federal DU Cell), is the western fraction of the Federal Cell. The eastern section is occupied by the 11e.(2) cell, which is dedicated to the disposal of uranium processing by-product waste, but not considered in this analysis. A stylized drawing of the Federal DU Cell and its relationship to the 11e.(2) cell is shown in Figure 1.

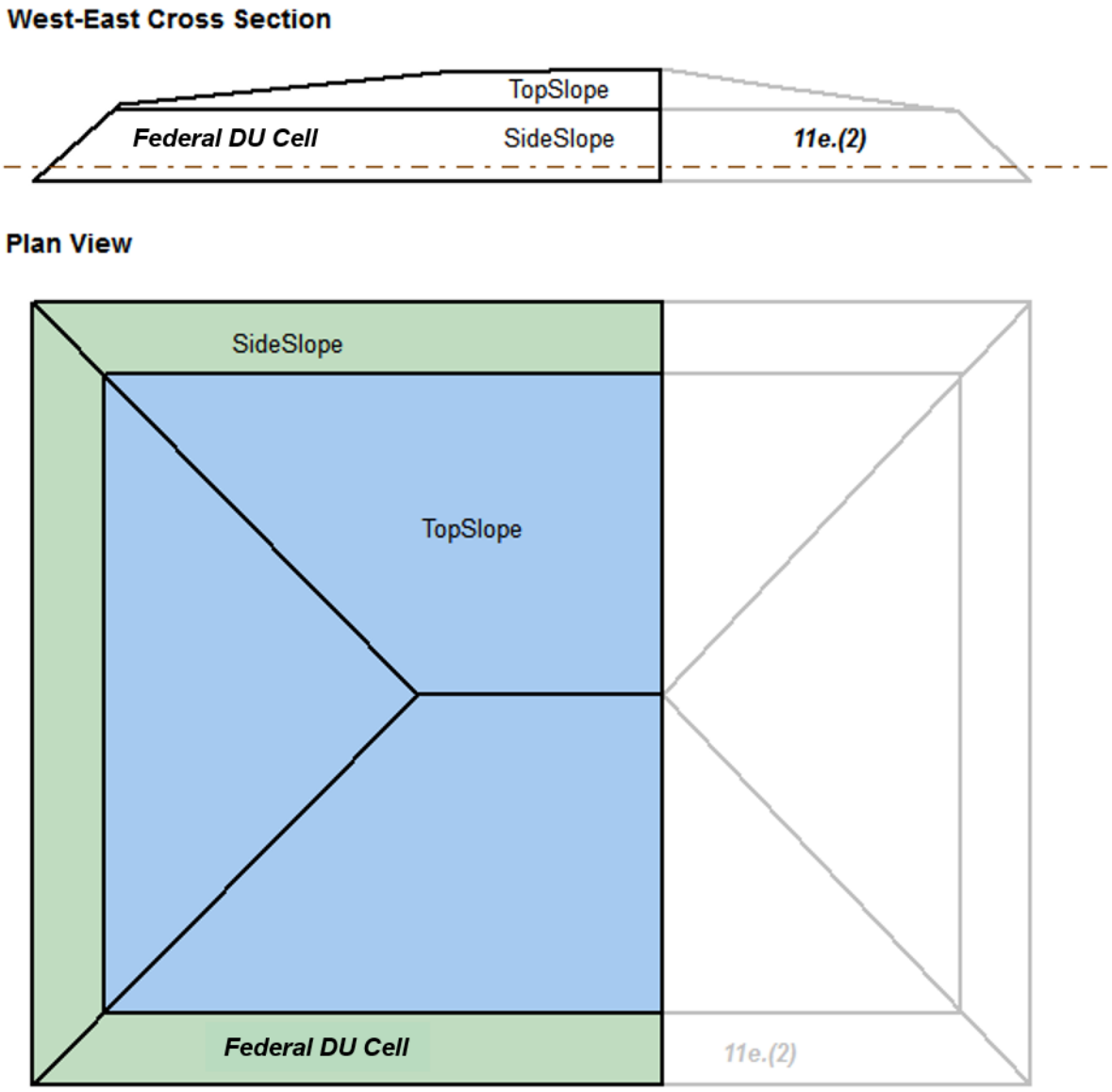

Figure 1. Section and Plan views of the the Federal DU Cell, with top slope shown in blue and side slope in green. The brown dotted line in the West-East Cross section represents below-grade (below the line) and above-grade (above the line) regions of the embankment.

The general aspect of the Federal DU Cell is that of a hipped cap, with relatively steeper sloping sides nearer the edges. The upper part of the embankment, known as the top slope, has a moderate slope, while the side slope is markedly steeper (20% as opposed to 2.4%). These two distinct areas, shown in different colors in Figure 1, are modeled separately in the Clive DU PA model. Each is built in GoldSim to be modeled as a separate one-dimensional column, with an area equivalent to the Federal DU Cell footprint. In the current Clive PA model, the sideslope portion of the model is inactive. The embankment is also constructed such that a portion of it lies

below-grade (Figure 1). The overall length of the embankment is 1430 ft and the overall width is 1775 ft. A detailed description of embankment dimensions and a discussion of representation of the Federal DU Cell in the GoldSim model are provided in the Embankment Modeling for the Clive DU PA Model white paper.

Disposal involves placing waste on a prepared clay liner that is approximately 8 ft below the ground surface. For the Federal DU Cell design, the depth of the waste below the top slope is a maximum of 53 ft (16 m). A cover system is constructed above the waste. The objective of the cover system is to limit contact of water with the waste. The cover is sloped to promote runoff and designed to limit water flow by increasing evapotranspiration (ET). The arrangement of the layers used for the ET cover design is shown in Figure 2. Beginning at the top of the cover the layers above the waste used for the ET cover design are:

- Surface layer: This layer is composed of native vegetated Unit 4 material with 15 percent gravel mixture on the top slope and 50 percent gravel mixture for the side slope. This layer is 6 inches thick. The functions of this layer are to control runoff, minimize erosion, and maximize water loss from ET. This layer of silty clay provides storage for water accumulating from precipitation events, enhances losses due to evaporation, and provides a rooting zone for plants that will further decrease the water available for downward movement.
- Evaporative Zone layer: This layer is composed of Unit 4 material. The thickness of this layer is 12 inches. The purpose of this layer to provide additional storage for precipitation and additional depth for plant rooting zone to maximize ET.
- Frost Protection Layer: This material ranges in size from 16 inches to clay size particles. This layer is 18 inches thick. The purpose of this layer is to protect layers below from freeze/thaw cycles, wetting/drying cycles, and inhibit plant, animal, or human intrusion.
- Upper Radon Barrier: This layer consists of 12 inches of compacted clay with a low hydraulic conductivity. This layer has the lowest conductivity of any layer in the cover system. This is a barrier layer that reduces the downward movement of water to the waste and the upward movement of gas out of the disposal cell.
- Lower Radon Barrier: This layer consists of 12 inches of compacted clay with a low hydraulic conductivity. This is a barrier layer placed directly above the waste that reduces the downward movement of water.

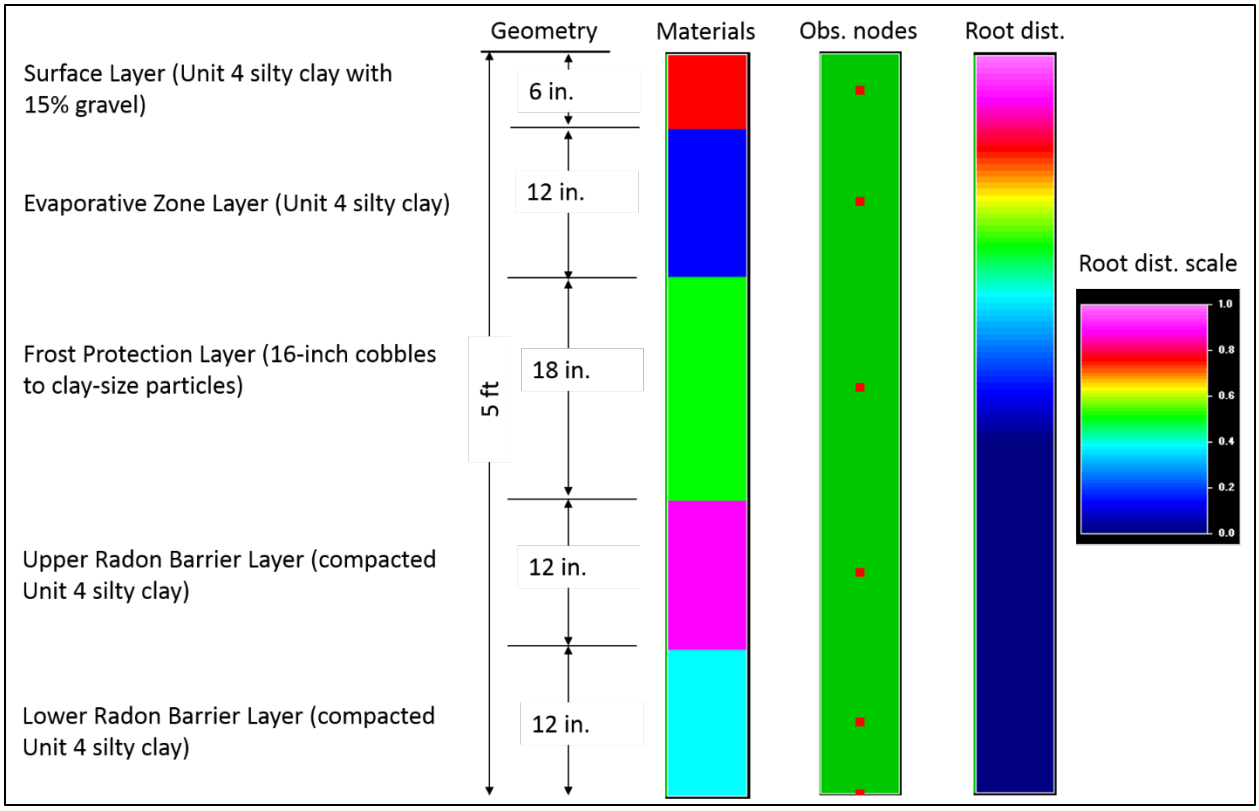

Figure 2. Evapotranspiration (ET) cover profile showing materials, observations nodes, and root distribution used in the HYDRUS-1D models.

4.0 Unsaturated Zone and Shallow Aquifer

The following description of the Clive site hydrology is taken from the review prepared by Envirocare (2004). The site is described as being located on lacustrine (lake bed) deposits associated with the former Lake Bonneville. The sediments underlying the facility are principally interbedded silt, sand, and clay. Sediments at the site are described by Bingham Environmental (1991, 1994) and Envirocare (2000, 2004) as being classified into four hydrostratigraphic units (HSU). Predominant sediment textural class, layer thickness range, and average layer thickness for each unit are listed in Table 3. A diagram of the unsaturated zone is shown in Figure 3.

Unit 4: This unit begins at the ground surface and extends to between 6 ft and 16.5 ft below the ground surface (bgs). The average thickness of this unit is 10 ft. This unit is composed of finer grained low permeability silty clay and clay silt.

Unit 3: Unit 3 underlies Unit 4 and ranges from 7 ft to 25 ft in thickness. The average thickness of this unit is 15 ft. Unit 3 is described as consisting of silty sand with occasional lenses of silty to sandy clay.

Unit 2: Unit 2 underlies Unit 3 and ranges from 2.5 ft to 25 ft in thickness. The average thickness of this unit is 15 ft. Unit 2 is described as being composed of clay with occasional silty sand interbeds. A structure map was prepared by Envirocare (2004, Figure 5) with contours

representing the elevations of the top of the unit. This map shows that the top surface of Unit 2 slopes downward gradually from east to west in the vicinity of the Class A South cell.

Unit 1: Unit 1underlies Unit 2 and is saturated beneath the facility, containing a locally confined aquifer. Unit 1 extends from approximately 45 ft bgs and contains the deep aquifer. The deeper aquifer is reported to be made up of lacustrine deposits consisting of deposits of silty sand with some silty clay layers. One or possibly more silty clay layers overlie the aquifer (Bingham Environmental 1994).

Table 3. Texture class, thickness range, and average thickness for the hydrostratigraphic units underlying the Clive site.

Unit	Sediment Texture Class	Thickness Range (ft)	Average Thickness (ft)
4	silt and clay	6 – 16.5	10
3	silty sand with interbedded silt and clay layers	7 - 25	15
2	clay with occasional silty sand interbeds	2.5 - 25	15
1	silty sand with interbedded clay and silt layers	>620	>620

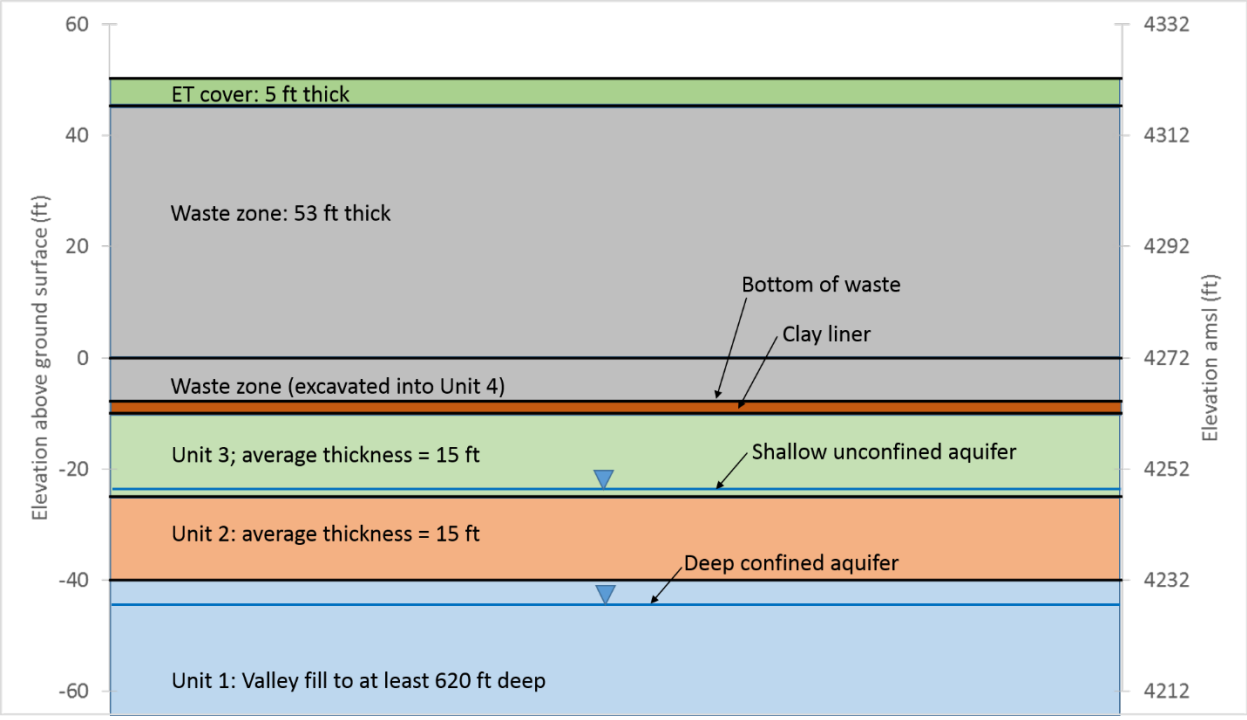

Figure 3. Stratigraphic profile showing ET cover, waste zone, and stratigraphy below the Federal DU Cell.

The aquifer system in the vicinity of the Clive Facility is described by Bingham Environmental (1991, 1994) and Envirocare (2000, 2004) as consisting of unconsolidated basin-fill and alluvial fan aquifers. Characterization of the aquifer system is based on subsurface stratigraphy

observations from borehole logs and from potentiometric measurements. The aquifer system is described as being composed of two aquifers; a shallow, unconfined aquifer and a deep confined aquifer. The shallow unconfined aquifer extends from the water table to a depth of approximately 40 ft to 45 ft bgs. The water table in the shallow aquifer is reported to be located in Unit 3 on the west side of the site and in Unit 2 on the east side.

The deep confined aquifer is encountered at approximately 45 ft bgs and extends through the valley fill (Bingham 1994). The boring log from a water supply well drilled in adjoining Section 29 indicated continuous sediments to a depth of 620 ft bgs (DWR 2014, water right number 16-816 and associated well log 11293). The deepest portion of the basin in the Clive area is believed to be north of Clive in Ripple Valley where the basin fill was estimated to be 3,000 ft thick (Baer and Benson (as cited in Black et al., 1999)).

Deeper saturated zones in Unit 1 below approximately 45 ft bgs are reported to show higher potentiometric levels than the shallow unconfined aquifer. Differences in potentiometric levels are attributed to the presence of the Unit 2 clays. These observations are interpreted as indicating that the shallow unconfined aquifer below the site does not extend into Unit 1 but is contained within Units 2 and 3 (Bingham Environmental, 1994). The aquifer systems are described in more detail in the Saturated Zone Modeling white paper.

Recharge to the shallow aquifer in the vicinity of Clive is thought to be composed of three components; a small amount due to vertical infiltration from the surface; some small amount of lateral flow from recharge areas to the east of the site; and the majority of recharge believed to be from upward vertical leakage from the deeper confined aquifer (Bingham Environmental, 1994). Average annual groundwater recharge from the surface in the southern Great Salt Lake Desert in the precipitation zone typical of Clive was estimated by Gates and Kruer (1981). An estimated 300 acre feet per year were recharged to lacustrine deposits and other unconsolidated sediments over an area of 47,100 acres. This is a recharge rate of approximately 0.08 inches/year.

Groundwater recharge from lateral flow occurs due to infiltration at bedrock and alluvial fan deposits away from the Site which moves laterally through the unconfined and confined aquifers (Bingham Environmental, 1994). This is evidenced by the increasing salinity of the groundwater due to dissolution of evaporate minerals as water moves from the recharge area to the aquifers below the Facility (Bingham Environmental, 1994). The majority of recharge to the shallow aquifer is believed by Bingham Environmental (1994) to be due to vertical leakage upward from the deep confined aquifer due to the presence of upward hydraulic gradients.

Deeper saturated zones in Unit 1 below approximately 45 ft bgs are reported to show higher potentiometric levels than the shallow unconfined aquifer. Differences in potentiometric levels are attributed to the presence of the Unit 2 clays (Bingham Environmental, 1994). Vertical gradients between shallow and deeper screened intervals in the monitor well clusters were calculated by Bingham Environmental (1994). An upward vertical gradient was observed ranging in magnitude from 0.02 to 0.04 based on the distance between the screen centers. For a vertical hydraulic conductivity of 1×10^{-6} cm/s (Bingham Environmental, 1994) this corresponds to a recharge range from 0.25 in/yr to 0.5 in/yr.

5.0 Climate

Precipitation measurements taken at the site over the 17-year period 1992 to 2009 show a mean annual value of 8.53 inches (21.7 cm) (Whetstone 2011). The distribution of precipitation throughout the year is shown in Figure 4. Precipitation exceeds the annual average from January through June and again in October and is below average for the remaining months. The nearest National Oceanographic and Atmospheric Administration (NOAA) station with a long-term record is located in Dugway, Utah approximately 40 miles to the south. The mean annual precipitation for the same 17-year period measured at the Dugway station is 8.24 inches (20.9 cm). A comparison of the Dugway precipitation data for the 17-year period 1992 to 2009 with the long-term average for Dugway was made by Whetstone (2011). This comparison indicated that annual average precipitation during this 17-year period has been greater than the long-term average at Dugway by 8 percent. Whetstone (2011) concluded that simulations of cover performance using precipitation data from this 17-year period might be overestimating this component of the site water balance.

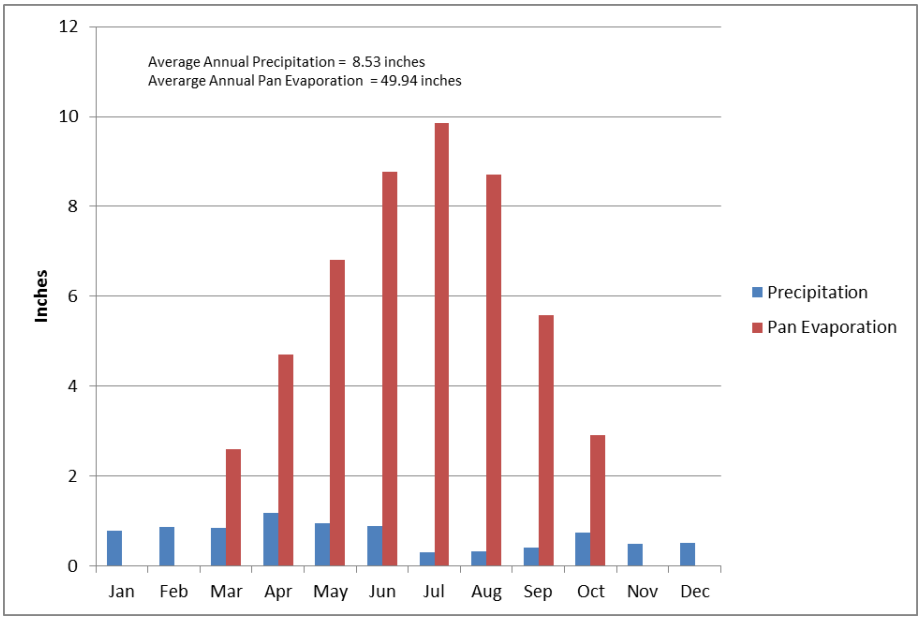

Figure 4. Monthly mean temperatures for the Clive Site and the NOAA BYU station at Provo, Utah.

The HYDRUS-1D modeling performed is based on the 17-year record for consistency with the modeling results reported in Whetstone (2011). However, an additional 2 years of monthly precipitation data are available from Meteorological Solutions (2012). The 19-year average precipitation is 8.62 inches (21.9 cm). This difference is driven primarily by the 4.28 inches of rainfall in May 2011. The small change in the overall average suggests that the modeling results presented for this analysis would not change significantly if the 19-year precipitation record had been used instead of the 17-year record.

The close correspondence between mean monthly temperatures measured at the Clive site and the Dugway NOAA station was demonstrated by Whetstone (2011). Average monthly

temperatures measured at the Clive site over the 17-year period 1992-2009 ranged from 27.7 ^{o}F in December to 79.5 ^{o}F in July.

Mean monthly values of pan evaporation measured at the BYU NOAA station in Provo, Utah over the period 1980 to 2005 are shown in Figure 5. Mean annual pan evaporation over this time period is 49.94 inches. This station is located 83 miles to the southeast of the Clive facility. Data from this station are used because pan evaporation data are not available for the Dugway station. Although the Clive site is warmer than Provo during the summer months as shown in Figure 4, the data provide insight into the water balance at the site.

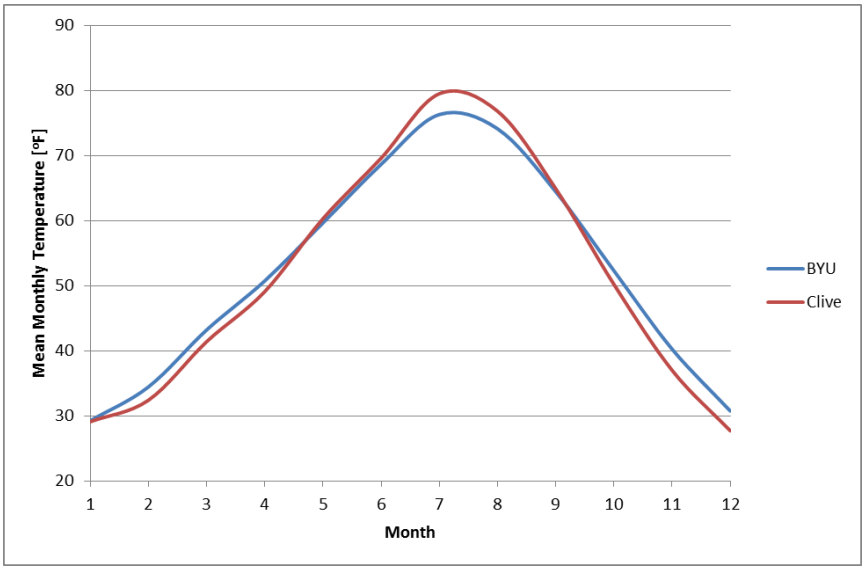

Figure 5: Monthly mean temperatures for the Clive Site and the NOAA BYU station at Provo, Utah.

Assuming pan evaporation is approximately equal to potential evapotranspiration (PET) the ratio of annual average precipitation to PET is 0.17. Although PET greatly exceeds precipitation on an annual basis, monthly means in Figure 4 show precipitation exceeds PET from November through February. This indicates the potential for recharge during these months under natural conditions at the site. This is only a coarse measure however that neglects other factors. Actual recharge is estimated through modeling of net infiltration.

6.0 Vegetation

Actual transpiration is dependent on the characteristics of the plant communities at the site. Vegetation cover at the site is less than 20 percent with soils supporting a range of native and invasive shrubs. Excavations at the site have shown plant rooting depths extending to approximately 31 inches (80 cm) below the ground surface with root density decreasing with depth (SWCA 2011).

Vegetation surveys of three field plots on or adjacent to the Clive Site were conducted by SWCA (2011). The three low desert vegetation associations were characterized as black greasewood, Plot 3; halogeton-disturbed, Plot 4; and shadscale-gray-molly, Plot 5. The dominant shrub in Plot

3 was black greasewood with a percent cover of 4.5% and the dominant forb was halogeton with a percent cover of 0.7%. In Plot 4 the dominant shrub was shadscale saltbush with a percent cover of 2.3% and the dominant forb was halogeton with a percent cover of 3.3%. In Plot 5 the dominant shrub was shadscale saltbush with a percent cover of 12.5% and the dominant forb was Halogeton with percent cover of 0.9%.

Black greasewood, shadscale saltbush, and halogeton are all classified as facultative halophytes (Anderson, 2004; Simonin, 2001; and Pavek, 1992). Facultative halophytes are known to benefit from high salt concentrations in their growth media (Shabala, 2013). Halophytes are able to adjust to saline environments through various physiological adaptations such as compartmentalization of ions in cell vacuoles, succulence, and the elimination of salt through salt-secreting glands and bladders (Shabala, 2013). Optimal growth for halophytes has been demonstrated by Shabala (2013) to occur in media with a concentration of approximately 50 mM NaCl for monocots, and between 100 and 200 mM for dicots. For the optimum range for dicots of 100 to 200 millimoles per liter (mM), the corresponding range of electrical conductivity for a NaCl solution is 9.7 to 18.3 mmho/cm (CRC, 1985).

Depending on the extent of the area defined on and adjacent to the Clive Site, approximately 80 to 90 percent of the soils are mapped as the Skumpah silt loam on 0 to 2 percent slopes (NRCS, 2013). This Unit is characterized as having maximum salinity ranging from 8.0 to 16.0 mmhos/cm. The top end of this range of maximum salinity does not exceed the maximum of the range of salinity considered optimum for halophyte growth of 18.3 mmho/cm. Given the similarity in ranges of salinity in the surface soils at the Clive Site and for optimum halophyte growth, the influence of the osmotic head reduction in the root-water uptake water stress response function is considered negligible and was, consequently, not included in the model.

7.0 Properties of Unit 3 and Unit 4

7.1 Laboratory Measurements

The hydraulic properties for Units 3 and 4 are based on laboratory measurements by the Colorado State University (CSU) Porous Media Laboratory for the moisture retention and hydraulic conductivity of core samples from Units 3 and 4 at the Clive site (Bingham Environmental, 1991). Measurements of water retention as a function of matric pressure (called suction head in this report) are available for the drying and wetting cycles. These measurements were performed on four cores: GW19A B1 and GW17A B2 from Unit 4 (a silty clay), and GW18 B4 and GW17A B5 from Unit 3 (a silty sand). Measurements of hydraulic conductivity as a function of moisture content are available for three cores: GW19A B1, GW18 B4, and GW17A B5. The focus in this work (and in previous work) is on the wetting cycle data because infiltration after rain, which is a major driver for downward flow and transport, is driven by a rewetting front that passes through the engineered cover, waste, and clay layers. The Appendix documents the hydraulic data for Units 3 and 4, based on data reported in (Bingham Environmental 1991, pp. B 19 through B 31).

7.2 Grain Size Distributions for the Cores

Tables 4 and 5 summarize the grain size distributions according to the Unified Soil Classification System (Bingham Environmental, 1991) for cores from Units 4 and 3, respectively. Table 4 is sorted by increasing percent of clay plus silt content. Table 5 is sorted by increasing percent of sand content. The four cores that were tested by CSU have the following properties:

- GW17A B2 has 55.6% clay, the highest measured clay content with a trace of sand in Table 4 for Unit 4,
- GW19A B1 has 56.2% silt, the highest measured silt content with a trace of sand in Table 4 for Unit 4,
- GW18 B4 has 45.5% sand, the lowest measured sand content in Table 5 for Unit 3, and
- GW17A B5 has 83.3% sand, the highest measured sand content in Table 5 for Unit 3.

The core samples that were selected for testing span the extremes of the clay, silt, and sand contents for Units 3 and 4. The core samples that were tested are in a bold font in Tables 4 and 5.

The water retention data are consistent with these material distributions, as shown in Figure 6. In particular, the core that has the greatest clay content retains a greater moisture content than the cores that are high in silt or sand at a given suction head, and the core that has the greatest sand content demonstrates the abrupt changes in moisture content that are typical of a sandy material.

Table 4. Grain size distributions for cores from Unit 4, a silty clay.

Well/Sample No.	Depth (ft)	Description	% Gravel	% Sand	% Silt	% Clay	% Clay + Silt	Reference
I-3-50 (SE)	1.5	Silty Clay	0	39.3			60.7	Bingham 1994, page 23
I-4-50 (SE)	10.5	Silty Clay	0	19.6			80.4	Bingham 1994, page 32
I-3-50 (SE)	10.5	Silty Clay	0	16.6			83.4	Bingham 1994, page 24
I-1-50 (NW)	7.5	Silty Clay	0	11.7			88.3	Bingham 1994, page 13
GW-16/S-1	3 - 5	Brown Silty Clay w/Trace Fine Sand	0.1	11.2	50.3	38.4	88.7	Bingham 1991, page B-13
GW-19A/S-1	**5-7**	**Brown Silty Clay w/Trace Fine Sand**	**0**	**2.8**	**56.2**	**41.0**	**97.2**	**Bingham 1991, page B-17**
GW-17A/L-2	**7-9.5**	**Brown Silty Clay w/Trace Fine Sand**	**0**	**2.1**	**42.3**	**55.6**	**97.9**	**Bingham 1991, page B-15**
GW-18/B-1	5-6.5	Brown Silty Clay w/Trace Fine Sand	0	2.0	49.9	48.1	98.0	Bingham 1991, page B-16
I-4-50 (SE)	7.5	Silty Clay	0	1.2			98.8	Bingham 1994, page 31

Cores in bold font were tested by CSU.

Table 5. Grain size distributions for cores from Unit 3, a silty sand.

Well/Sample No.	Depth (ft)	Description	% Gravel	% Sand	% Silt	% Clay	% Clay + Silt	Reference
GW-18/S-4	**20-22**	**Brown Silty Fine Sand w/Some Clay**	**0**	**45.5**	**38.7**	**15.8**	**54.5**	**Bingham 1991, page B-16**
I-1-50 (NW)	18.0	Silty Sand	0	48.2			51.8	Bingham 1994, page 15
DH-48/B-2	17-19	Tan Silty Sand	0	55.5			44.5	Bingham 1994, page B-11
GW-16/B-4	19.5-21	Tan Silty Fine Sand	0	59.4			40.6	Bingham 1991, page B-14
I-3-50 (SE)	19.5	Silty Sand	0	62.3			37.7	Bingham 1994, page 26
GW-41/B-6	10-12	Tan Silty Sand	0	65.3			34.7	Bingham 1994, page B-10
GW-41/B-9	16-18	Tan Silty Sand	0	66.3			33.7	Bingham 1994, page B-10
I-1-50 (NW)	10.5	Silty Sand	0	66.6			33.4	Bingham 1994, page 14
GW-19B/B-4	17-19	Tan Silty Fine Sand	0	66.7			33.3	Bingham 1991, page B-18
GW-55/B-8	14-16	Tan Silty Sand	1.1	69.5			29.4	Bingham 1994, page B-11
DH-33/L-7	16.5	Tan Silty Sand	0.1	72.9			27	Bingham 1994, page B-9
GW-16/B-3	14.5-16	Tan Silty Fine Sand	0.2	74.7			25.1	Bingham 1991, page B-13
I-3-50 (SE)	15	Silty Sand	0	75.8			24.2	Bingham 1994, page 25
I-4-50 (SE)	21	Silty Sand	0	76.4			23.6	Bingham 1994, page 33
GW-16/B-2	9.5-11	Tan Silty Fine Sand	1.6	79.8			18.6	Bingham 1991, page B-13
GW-19A/S-3	15-16	Brown Silty Fine	0	82.0			18	Bingham 1991,

Well/Sample No.	Depth (ft)	Description	% Gravel	% Sand	% Silt	% Clay	% Clay + Silt	Reference
		Sand						page B-17
GW-17A/L-5	**19.5-22**	**Brown Silty Fine Sand w/Trace Clay**	**0**	**83.8**	**8.4**	**7.8**	**16.2**	**Bingham 1991, page B-15**
GW-19B/L-5	22-24.5	Tan Silty Fine Sand	0	83.8			16.2	Bingham 1991, page B-18

Cores in bold font were tested by CSU.

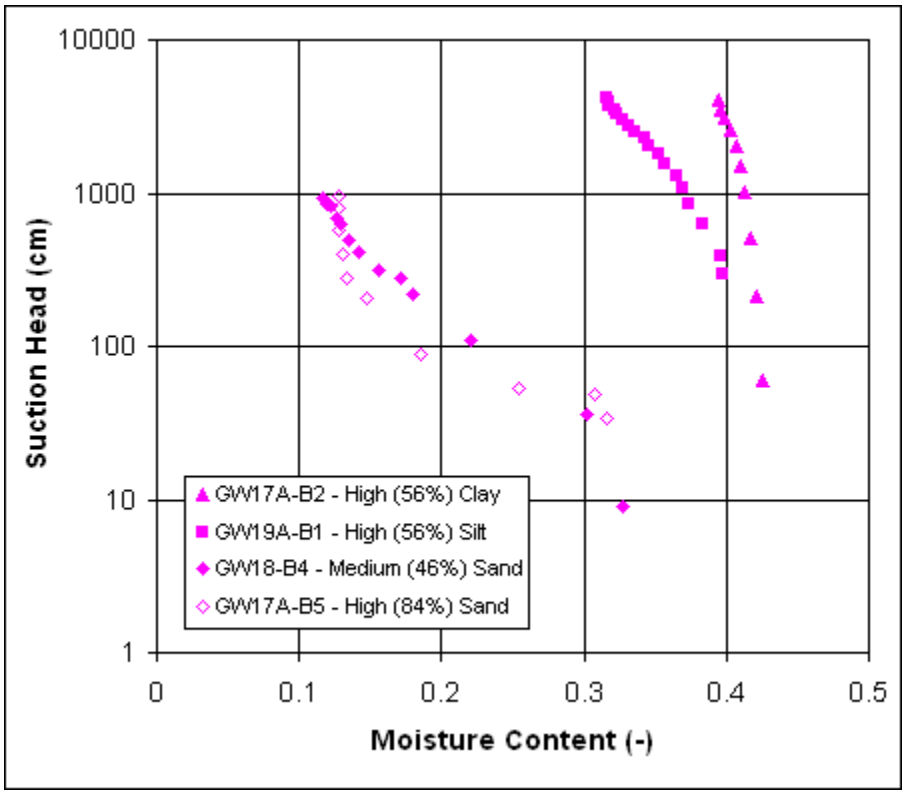

Figure 6. Comparison of water retention data (wetting cycle) for four core samples

7.3 Soil Material Properties

Particle density ρ_s is defined as the ratio of the mass of the solid to the volume of the solid:

$\rho_s = M_{solid} / V_{solid}$.

Particle density depends on the chemical composition and crystalline structure of the mineral particles. Particle density is not influenced by particle size, packing arrangement, or pore space.

Dry bulk density ρ_b is defined as the ratio of the mass of dried alluvium to its total volume,

$\rho_b = M_{solid} / V_{total}$.

For a dried sample, $V_{total} = V_{solid} + V_{gas}$.

Porosity, ϕ, (often also denoted as n) is the relative pore volume of the medium,

$(V_{liquid} + V_{gas}) / (V_{solid} + V_{liquid} + V_{gas})$.

For a dry sample, porosity is $V_{gas} / (V_{solid} + V_{gas})$. Total porosity can be determined from dry bulk density and particle density by $\phi = 1 - \rho_b / \rho_s$. Therefore, relating these equations,

$\phi = 1 - \rho_b / \rho_s = (\rho_s - \rho_b)/\rho_s = [M_{solid} / V_{solid} - M_{solid} / (V_{solid} + V_{gas})] / (M_{solid}/V_{solid} = V_{gas} / (V_{solid} + V_{gas})$.

The structure of coarse dry alluvium is generally single grained. The actual packing arrangement depends on grain size distribution, grain shape, and the processes under which the alluvium was deposited. The grain size distribution can consist of a single grain size (monodisperse) or multiple grain sizes (polydisperse). The packing arrangements of spherical grains of uniform size can be represented by models for regular packing that allow the calculation of the spacing of layers, the volume of a unit cell and thus the bulk density. Although monodisperse systems are idealizations of natural porous materials such as alluvium, calculated relationships between particle density and bulk density gives some insight into potential particle density – bulk density correlation. The unit cell volume, bulk density, and porosity are given in Table 6 below for five models of regular packing of uniform spheres.

Table 6. Theoretical porosities based on particle packing geometry.

Model	Unit Cell Volume (R is grain radius)	Bulk Density	Porosity
simple cubic	$8R^3$	$\pi\rho_s/6$	47.64
cubic tetrahedral	$4\sqrt{3}\ R^3$	$\pi\rho_s/3\sqrt{3}$	39.54
tetragonal sphenoidal	$6R^3$	$2\ \pi\rho_s/9$	30.19
pyramidal	$4\sqrt{2}R^3$	$\pi\rho_s/3\sqrt{2}$	25.95
tetrahedral	$4\sqrt{2}R^3$	$\pi\rho_s/3\sqrt{2}$	25.95

These calculations show that the bulk density of a volume of monodisperse spheres of constant particle density depends on the packing arrangement. Thus, correlation between particle density and bulk density would only be expected for a sample characterized by a single packing arrangement.

Polydisperse systems are more complex with grains of smaller radii filling in the pore spaces between larger grains. The increase in bulk density due to infilling by smaller particles depends

on the grain size distribution. Natural materials are more likely to be characterized by a range of particle sizes leading to many diverse packing arrangements. The large range of possible packing arrangements in coarse alluvium makes a physically based correlation between particle density and bulk density unlikely.

Given the conclusion that particle density and bulk density are not physically dependent and given the need to restrict the sampling of material properties and moisture content parameters to physically meaningful and consistent values the following approach was taken:

1. Separate up-scaled distributions for Unit 3 and 4 for saturated water content and residual water content are estimated from borehole water retention curve and hydraulic conductivity data. This estimation approach is detailed in subsequent sections.

2. Porosity is assumed to be equal to the saturated water content.

3. Based on particle density data presented in Table 7 and best professional judgment a constant value of 2.65 g/cm3 was chosen for particle density for both Units 3 and 4, and the frost protection layer.

4. Based on bulk density data presented in Table 7 and best professional judgment an up scaled distribution for bulk density was specified as a normal distribution with a mean of (1- porosity) times particle density and a standard deviation of 0.1. This was applied to both Units 3 and 4, and the frost protection layer.

This approach allows the uncertainty in water content and bulk density to be modeled while maintaining a physically coherent probabilistic unsaturated zone model.

Table 7. Bulk density, porosity, and calculated particle density data from water retention experiments.

Borehole	Unit	Bulk Density (g/cm)	Porosity	Calculated Particle Density (g/cm^3)
GW18-B4	3	1.567	0.409	2.65
GW17A-B5	3	1.673	0.32	2.46
GW19A-B1	4	1.397	0.473	2.65
GW17A-B2	4	1.326	0.505	2.68

from CSU Porous Media Laboratory

7.4 Soil Moisture Content

The flow of water in porous media occurs in response to a gradient in the total potential energy of water. The total potential can be composed of a number of components but this analysis will

be restricted to gravitational and matric potentials. Water potential components are often expressed in units of energy per unit weight rather than units of energy per unit mass. When the quantity of water is expressed as a weight, the units of potential are defined in terms of head. The gravitational potential refers to the energy of water with respect to reference elevation and is written here as Z. Although not a formal definition, the matric potential relates to the energy of the tension imposed on the pore water by the soil matrix. Matric potential is a negative value and is written here as ψ. The total potential is then H = ψ + Z.

Steady-state fluid flow in an unsaturated medium is defined by the Buckingham-Darcy equation (Jury and Horton, 2004, p.95). In the following discussion this equation will be referred to simply as the Darcy equation. The one dimensional form of Darcy's equation for unsaturated flow is given by Fayer (2000, Eqns. 4.2 and 4.5):

$$q = -K_L(\psi)\frac{\partial H}{\partial z} \tag{1}$$

where

q	is the flux of liquid per unit area,
K_L	is the unsaturated conductivity as a function of the matric head ψ,
H	is the matric plus gravitational potentials [cm], and
z	is the depth below ground surface [cm].

It is convenient to define two sign conventions for the total potential (Fayer 2000, page 4.2): (1) the *z*-coordinate is zero at the soil surface and positive downward. With this convention, the gravitational head in the soil, which is defined as the elevation of a point with respect to the soil surface, and negative and defined as -*z*; and (2) the suction head, *h*, is the negative of the matric potential or matric head, ψ. With this convention, the suction head, *h*, is always greater than zero for an unsaturated soil. It follows that

$$H = \psi + Z = -(h + z) \tag{2}$$

and the flux is then given by

$$q = K_L(h)\left(\frac{\partial h}{\partial z} + 1\right) \tag{3}$$

The unsaturated conductivity, K_L, is formulated based on the Brooks-Corey representation for moisture content as a function of suction head

$$\begin{aligned} \Theta &= \left(\frac{h}{h_b}\right)^{-\lambda} \quad \text{for} \quad h > h_b \\ &= 1 \quad \text{for} \quad 0 \le h \le h_b \end{aligned} \tag{4}$$

where

Θ	is the effective saturation,
h	is the suction head (cm),

h_b is the bubbling pressure head (cm) at which moisture first drains from the material, and

l is a constant that is fit to data.

Alternatively, expressed in terms of the fractal dimension, D

$$\Theta = \left(\frac{h}{h_b}\right)^{D-3} \quad \text{for} \quad h > h_b$$
$$= 1 \quad \text{for} \quad 0 \le h \le h_b \tag{5}$$

The suction head is positive for an unsaturated material and 0 at saturation. Θ, the effective saturation, is defined as

$$\Theta = \frac{\theta - \theta_r}{\theta_s - \theta_r} \tag{6}$$

where

θ is the moisture content,

θ_r is the residual moisture content, and

θ_s is the saturated moisture content.

Combining Equations

$$\theta = \theta_r + (\theta_s - \theta_r)\left(\frac{h}{h_b}\right)^{-\lambda} \tag{7}$$

This equation can then be fit to core data.

Alternatively, expressing in terms of D and assuming

$$\theta = \theta_r + (\theta_s - \theta_r)\left(\frac{h}{h_b}\right)^{D-3} \tag{8}$$

Using the Mualem theory for predicting hydraulic conductivity (Mualem 1976), the unsaturated hydraulic conductivity is defined as

$$K_L = K_S \Theta^{2+\frac{2}{\lambda}} \tag{9}$$

Substituting Equation 6 into Equation 9 gives:

$$K_L = K_S \left(\frac{\theta - \theta_r}{\theta_s - \theta_r}\right)^{2+\frac{2}{\lambda}} \tag{10}$$

Setup (e.g. unit 3)

1) from 4 measurements estimate mean and standard error for porosity (ϕ) and θ_r, use these as priors for θ_s and θ_r (assumes $\theta_s = \phi$).

2) for each borehole core there are 2 separate measurements

1. moisture content, θ; and suction head, h
2. moisture content, θ; and hydraulic conductivity K_L
3. estimate h_b, D, θ_s, θ_r, and K_s as described below

Here's the Brooks-Corey $\theta \sim f(h)$ equation:

$$\theta = \theta_r + (\theta_s - \theta_r)\left(\frac{h}{h_b}\right)^{(D-3)} \tag{11}$$

Here's $K_L \sim f(\theta)$

$$K_L = K_S\left(\frac{\theta - \theta_r}{\theta_s - \theta_r}\right)^{-(\tau+2/(D-3))} \tag{12}$$

where the data are

θ	the water content,
h	is the suction head (cm),
K_L	is hydraulic conductivity (cm/sec),

and the parameters to be fit are

h_b	is the air entry pressure head (cm),
D	is the soil fractal dimension,
θ_s	is the saturated water content,
θ_r	is the residual water content,
τ	is the Mualem empirical parameter = 2,
K_S	is saturated hydraulic conductivity (cm/sec).

Typically these relationships are fit using non-linear least squares. However, it seems for these boreholes the optimization has trouble converging and the uncertainty in parameter estimates is difficult to estimate. To allow combining of information available across the available borehole moisture content and hydraulic conductivity datasets and to provide an estimate of the uncertainty in these parameter estimates a Bayesian Markov Chain Monte Carlo (MCMC) simulation approach was taken that allows the parameters to be constrained via prior distributions and generates parameter posterior distributions. This also allows the two sets of information from a borehole to be combined as well as allowing for combining information across boreholes for a unit (borehole data are presented in the Appendix).

In a Bayesian approach sources of information on model parameters can be combined through a prior distribution or through a data likelihood. The priors integrate expert judgment and scientific knowledge while the likelihood integrates information available in observed data. In effect, the priors can be used to constrain the results parameter distribution to physical meaningful values.

The priors listed below (Equations 13-19) are all non-informative distributions which allow the data to determine the distribution and also constrain the parameter values to a physically meaningful range.

$$p(\theta_s) = U[0.3,0.55] \tag{13}$$

$$p(\theta_r) = U[0.001,0.2] \tag{14}$$

$$p(h_b) = U[1,500] \tag{15}$$

$$p(D) = U[1,2.999] \tag{16}$$

$$p(\sigma) = U[0.001,1000] \tag{17}$$

$$p(K_s) = U[10\mathrm{e}-10,10\mathrm{e}-3] \tag{18}$$

$$p(\sigma_{K_S}) = U[1\mathrm{e}-91\mathrm{e}-4] \tag{19}$$

and the likelihood based on the moisture content matrix pressure data:

$$\begin{aligned} p(\theta_s, h_b, D, \sigma | \theta_{borehole1}, \theta_{borehole2}, h_{borehole1}, h_{borehole2}) = \\ N_{borehole1}\left[\theta_r + (\theta_s - \theta_r)\left(\frac{h_{borehole1}}{h_b}\right)^{(D-3)}, \sigma\right] \\ N_{borehole2}\left[\theta_r + (\theta_s - \theta_r)\left(\frac{h_{borehole2}}{h_b}\right)^{(D-3)}, \sigma\right] \end{aligned} \tag{20}$$

and the likelihood based on the moisture content hydraulic conductivity data:

$$\begin{aligned} p(\theta_s, \theta_r, D, K_S, \sigma_{K_S} | \theta_{borehole1}, \theta_{borehole2}, K_{L_{borehole1}}, K_{L_{borehole2}}) = \\ N_{borehole1}\left[K_S\left(\frac{(\theta - \theta_r)}{(\theta_s - \theta_r)}\right)^{-(2+2/(D-3))}, \sigma_{K_S}\right] \\ N_{borehole2}\left[K_S\left(\frac{(\theta - \theta_r)}{(\theta_s - \theta_r)}\right)^{-(2+2/(D-3))}, \sigma_{K_S}\right] \end{aligned} \tag{21}$$

Markov Chain Monte Carlo (MCMC) simulation of the joint distribution define by equations 13-21 was used to generate samples from the marginal parameter distributions for the moisture content and hydraulic conductivity models. Results for Unit 3 and 4 are presented in the following sections.

7.4.1 Unit 3 Brooks-Corey Parameters

The MCMC sampling using likelihoods incorporating the two Unit 3 borehole cores resulted in the the following marginal parameter distributions:

$$p(h_b) = N[mean = 8.85, sd = 0.929] \quad (22)$$

$$p(D) = N[mean = 2.73, sd = 5.21\text{e} - 3] \quad (23)$$

$$p(K_S) = N[mean = 5.14\text{e} - 05, sd = 5.95\text{e} - 6] \quad (24)$$

$$p(\theta_s) = N[mean = 0.393, sd = 6.11\text{e} - 03] \quad (25)$$

$$p(\theta_r) = N[shape = 6.78\text{e} - 3, scale = 2.05\text{e} - 3] \quad (26)$$

Significant correlations from these simulations was found between D and h_b (-0.85) and between K_s and D (-0.98).

7.4.2 Unit 4 Brooks-Corey Parameters

The MCMC sampling using likelihoods incorporating the two Unit 4 borehole cores resulted in the the following marginal parameter distributions:

$$p(h_b) = N[mean = 104., sd = 1.72] \quad (27)$$

$$p(D) = N[mean = 2.81, sd = 9.93\text{e} - 5] \quad (28)$$

$$p(K_S) = N[mean = 5.16\text{e} - 05, sd = 5.97\text{e} - 7] \quad (29)$$

$$p(\theta_s) = N[mean = 0.428, sd = 9.08\text{e} - 3] \quad (30)$$

$$p(\theta_r) = N[shape = 0.108, scale = 8.95\text{e} - 4] \quad (31)$$

Significant correlations from these simulations was found between D and h_b (-0.66) and between K_s and D (-0.37).

8.0 Properties of Radon Barriers

The Radon Barrier layers are divided into upper and lower layers. Both are constructed of local Unit 4 silty clay, compacted to different hydraulic conductivities. UpperRnClay represents the upper of the two layers and LowerRnClay represents the lower of the two layers.

9.0 Properties of Waste

Test data are not available for the unsaturated porous media properties of the wastes. However, the DU waste is expected to be in a powdered form or possibly compressed into small "briquettes" for safety during transportation to the Clive facility. In this condition, the DU waste will behave like a mixture of fine sand to fine gravel. Since there is so little information on which to base material properties for the waste, it is assigned the properties of Unit 3.

Three types of waste materials are considered in the DU PA: Generic LLW, the UO3 waste from the SRS, and the U3O8 wastes from the gaseous diffusion plants (GDPs) at Portsmouth, OH, and Paducah KY. The generic LLW is used only as an inert filler in the model, with no inventory, and is assumed to simply have the properties of local silty sandy soil: Unit 3.

The uranium oxide wastes, both UO3 and U3O8, will be disposed in an indeterminate mix of materials, including containers (55 gallon drums and DU cylinders of various types) and possibly concrete, grout, bulk LLW, and local soils as backfill. This complex mix of heterogeneous materials is not modeled at this point, and the assumption is made instead that the overall material properties are again simply that of local silty sandy soil: Unit 3.

So, in summary, all waste materials in the Clive DU PA Model are assumed to have the same physical properties as Unit 3 soils.

10.0 Properties of the Clay Liner

The Liner is constructed of compacted local clay, here defined as LinerClay. Distributions for the liner clay parameters are described in Table 1. The distribution for saturated hydraulic conductivity was developed using the design value from Table 8 of Whetstone (2007) for the clay liner of 1×10^{-6} cm/s as the geometric mean of a lognormal distribution. A geometric standard deviation of 1.2 was chosen to provide an approximate order of magnitude variation above and below the geometric.

11.0 Properties of the Unsaturated Zone below the Clay Liner

The Federal DU Cell is constructed by excavating through Unit 4, and into the top of Unit 3. The entire unsaturated zone below the embankment, from the bottom of the clay liner to the top of the saturated zone, is modeled as Unit 3 material, sharing all the properties and characteristics of Unit 3 as outlined in this white paper. The saturated zone is modeled as Unit 2 (see the Saturated Zone Modeling white paper). In the GoldSim PA Model, this zone below the embankment is called the “Unsat zone”, and does not include overlying waste and cover materials. It is part of both the top slope and side slope columns.

The thickness of the Unsat zone below the Federal DU Cell is determined by the difference in average elevations of the bottom of the clay liner and the water table. The clay liner is uniformly about 60 cm (2 ft)-thick by design, though the bottom of the waste cell has a gentle slope to it, as documented in the Embankment Modeling white paper.

A distribution for the thickness of the unsaturated zone was established based on measurements for groundwater wells, engineering drawings for the Federal DU Cell (see the Embankment Modeling white paper), and consideration of the accuracy of the elevation measurements. The four wells are selected from a map of wells (Figure 7 in Bingham Environmental, 1991): GW 19A, GW 25, GW 27, and GW-60, since the location of these four wells bound the Class A waste cell. Each groundwater well is in the vicinity of one of the four corners of the Federal DU Cell, so their measurements are treated as approximations to the water table elevation at the four corners. These water table elevations are also used to establish the distributions for the thickness of the saturated zone, and are documented in the Saturated Zone Modeling white paper.

12.0 Modeling of Net Infiltration and Water Content for the Clive DU PA Model

Steady-state water infiltration rates and water contents for the cover layers required as input for the Clive DU PA GoldSim model were calculated from a regression model developed from infiltration modeling using the HYDRUS-1D software package. This section describes the abstraction of the HYDRUS-1D results into the probabilistic framework employed by GoldSim.

12.1 Description of HYDRUS

HYDRUS-1D was selected for simulating the performance of the ET cover proposed for the DU waste cell. The HYDRUS-1D platform was selected for this project because of its ability to simulate processes known to have a significant role in water flow in landfill covers in arid regions. HYDRUS includes the capabilities to simulate:

- water flow in variably-saturated porous media,
- material hydraulic property functions,
- atmospheric surface boundary conditions including precipitation and evapotranspiration,
- root water uptake, and
- free-drainage boundary conditions.

The flow component of unsaturated flow and transport software packages with atmospheric boundary conditions such as HYDRUS solve modified forms of the Richards equation for variably saturated water flow. The flow equation incorporates a sink term to account for water uptake by plant roots. HYDRUS can be applied to one-, two-, and three-dimensional problems. The HYDRUS software includes grid generators for structured and unstructured finite element meshes. Programs such as HYDRUS require detailed data to represent the atmospheric boundary conditions and plant responses that are the dominant influences on flow in the cover in arid and semi-arid conditions. These programs use the infiltration capacity of the soil at any time as calculated in the model to partition precipitation into infiltration and overland flow. HYDRUS has been used for many applications for unsaturated zone modeling and has received numerous favorable reviews such as Scanlon's (2004) review of HYDRUS-1D, Diodato's (2000) review of HYDRUS-2D and McCray's (2007) review of the most recent program, HYDRUS (2D/3D).

HYDRUS-1D was selected for simulating flow in the Federal DU cell ET cover since previous numerical modeling of flow in the similar ET cover design for the Class A West cover demonstrated that subsurface lateral flow was not significant (Energy*Solutions*, 2012). To test the importance of 2-D flow effects in the ET cover design 2-D transient flow simulations were conducted for representative sections of the cover. The approach taken was to model a section of the side slope in two-dimensions. Representative hydraulic properties were assigned to the ET cover layers and the models were run with daily atmospheric boundary conditions for 100 years. Root water uptake was modeled assuming the roots extended to the bottom of the evaporative zone layer and a rooting density that decreased with depth.

The results of these 2-D simulations demonstrated that water flow in the cover system for both designs is predominantly vertical with no significant horizontal component. These results

demonstrate that 1-D models can be used to provide a defensible analysis of cover performance for the ET cover design due to the lack of lateral flow.

HYDRUS-1D models were developed for the evapotranspiration cover designs for the DU waste cell (Figure 2). Model development requires construction of a computational grid based on the geometry of the model domain. Hydraulic properties for each layer required for the model are available from previous studies at the site or can be estimated from site-specific measurements such as particle size distributions. HYDRUS requires daily values of precipitation, potential evaporation, and potential transpiration to represent the time-variable boundary conditions on the upper surface of the cover. Representative boundary conditions were developed from records of nearby meteorological observations. Parameters for describing root water uptake were available from the literature.

HYDRUS implements the soil-hydraulic functions of van Genuchten (1980) who used the statistical pore-size distribution model of Mualem (1976) to obtain a predictive equation for the unsaturated hydraulic conductivity function in terms of soil water retention parameters. The expressions of van Genuchten (1980) are given by

$$\theta(h) = \begin{cases} \theta_r + \dfrac{\theta_s - \theta_r}{[1+|\alpha h|^n]^m} & h < 0 \\ \theta_s & h \geq 0 \end{cases} \tag{32}$$

$$K(h) = K_s S_e^l [1 - \left(1 - S_e^{\frac{1}{m}}\right)^m]^2 \tag{33}$$

where

$$m = 1 - 1/n, \qquad n > 1 \tag{34}$$

The above equations contain five independent parameters: θr, θs, α, n, and K_s. The pore-connectivity parameter "l" (lower-case L) in the hydraulic conductivity function was estimated (Mualem, 1976) to be about 0.5 as an average for many soils. The value for l is commonly taken to be 0.5, and this value was used for all simulations for all soil types. The effective saturation, Se, is identical to Θ in Equation 6.

12.2 Conceptual Model

Recharge is an important process in controlling the release of contaminants to the groundwater pathway. Site characteristics influencing movement of water from precipitation through the vadose zone to the water table at the Clive site include climate, soil characteristics, and native

vegetation. Engineered barriers are used at the Clive site to control the flow of water into the waste. A hydrologic model of the waste disposal system must realistically represent precipitation, the source of water to the system, runoff, evaporation, transpiration, and changes in storage to estimate the flow through the system. Under natural conditions plants remove water from the upper soil zone through root uptake and transpiration reducing the water available for seepage deeper into the profile. The same processes occur in an engineered cover layer that has been revegetated. Seepage through a cover system can occur when soils become wet enough to increase their conductivity to water. Cover surface layers with adequate storage capacity can hold the water in the near surface until it can move back into the atmosphere through evaporation reducing the seepage of water to the waste. These processes would be expected to show temporal variability at the Clive site on the time scale of minutes to hours in the near surface and days to years deeper in the disposal cell. With time, cover properties may change from as-built conditions to more "naturalized" conditions due to plant and animal activity and climate influences (e.g. frost heave, erosion).

12.3 Climate and Vegetation Parameters

Infiltration of precipitation, surface runoff, and evaporation under time-varying climate conditions are modeled by HYDRUS. The data required includes daily values of precipitation, potential evaporation, and potential transpiration to represent the time-variable boundary conditions on the upper surface of the cover. The location of nearby meteorological stations and the time period of available records were discussed in Section 5. The long-term evaluation period for this analysis makes it necessary to generate a representative climate record with a longer term than the existing data.

The WGEN model (Richardson and Wright 1984) was used to generate a 100-year synthetic precipitation record for the site. The WGEN model is a component of the HELP model (Schroeder et al. 1994a, 1994b). A 100-year precipitation record was generated using the monthly average values from measurements at the site based on 17 years of observations. This 100-year record is shown in Figure 7. The annual mean was 8.42 inches (21.38 cm/yr) with a maximum daily precipitation of 1.09 inches (2.77 cm).

Daily potential evapotranspiration (PET) was calculated with values of daily maximum (T_{max}), minimum (T_{min}), and mean (T_{mean}) temperatures and extraterrestrial radiation using the Hargreaves method (Neitsch et al. 2005). This approach is used extensively and is documented in the HYDRUS manuals (Šimůnek et al. 2009). Using the Hargreaves method, PET is calculated as

$$\lambda E_0 = 0.0023 \cdot H_0 \cdot (T_{\max} - T_{\min})^{1/2} \cdot (\overline{T}_{mean} + 17.8) \tag{35}$$

where

λ = latent heat of vaporization [MJ kg^{-1}]

E_0 = potential evapotranspiration [mm d^{-1}]

H_0 = extraterrestrial radiation [MJ m^{-2} d^{-1}]

T_{max} = maximum air temperature for the day [°C]

T_{min} = minimum air temperature for the day [°C]

T_{mean} = mean temperature for the day [°C].

Monthly mean values for T_{max} and T_{min} based on a 30-year record are available from the Dugway, Utah NOAA station (WRCC 2012). Monthly average temperatures were used from this long-term record in HELP to provide daily 100-year records for T_{max} and T_{min}. T_{max} ranged from 14.7 to 110.7°F with a mean of 66.4 °F. T_{min} ranged from -9.1 to 75.3°F with a mean of 36.5°F. T_{mean} ranged from 2.8 to 93°F with a mean of 51.4°F. Daily maximum and minimum air temperatures for a 100-year record is shown in Figure 8. Daily PET values for a 100-year record were then calculated from these temperature data using the Hargreaves method described above. The daily 100-year PET record is shown in Figure 9.

The HYDRUS atmospheric boundary condition requires that potential soil evaporation and potential transpiration be specified separately. Potential evaporation (E_p) and potential transpiration (T_p) can be calculated from PET using the Beer-Lambert law (Varado et al. 2006; Wang et al. 2009). This calculation requires an estimate of the vegetation leaf area (LAI) index. The leaf area index is the one-sided active leaf area per unit ground surface area. Using the Beer-Lambert law

$$\begin{aligned} T_p &= PET \cdot (1 - \exp(-a_{bl} \cdot LAI)) \\ E_p &= PET \cdot \exp(-a_{bl} \cdot LAI) \end{aligned} \tag{36}$$

Where the a_{bl} coefficient accounts for radiation intercepted by vegetation and is given the default value of 0.5 (Varado et al. 2006).

A single LAI value of 0.082 was used for all the HYDRUS-1D simulations. This value was provided by Goodman (1973) for the total yield (all spp.) for a mixed vegetation plot for the month of April. The Goodman (1973) study was located in the Curlew Valley, UT portion of the glacial Lake Bonneville, located approximately 75 miles north of the Clive site.

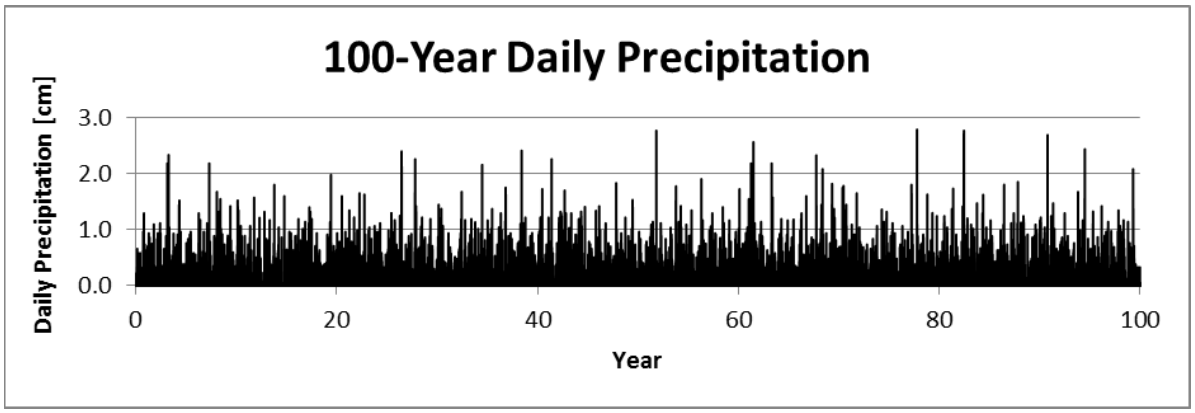

Figure 7. 100-year daily precipitation record generated from monthly average values of daily measurements at the site based on 17 years of observations.

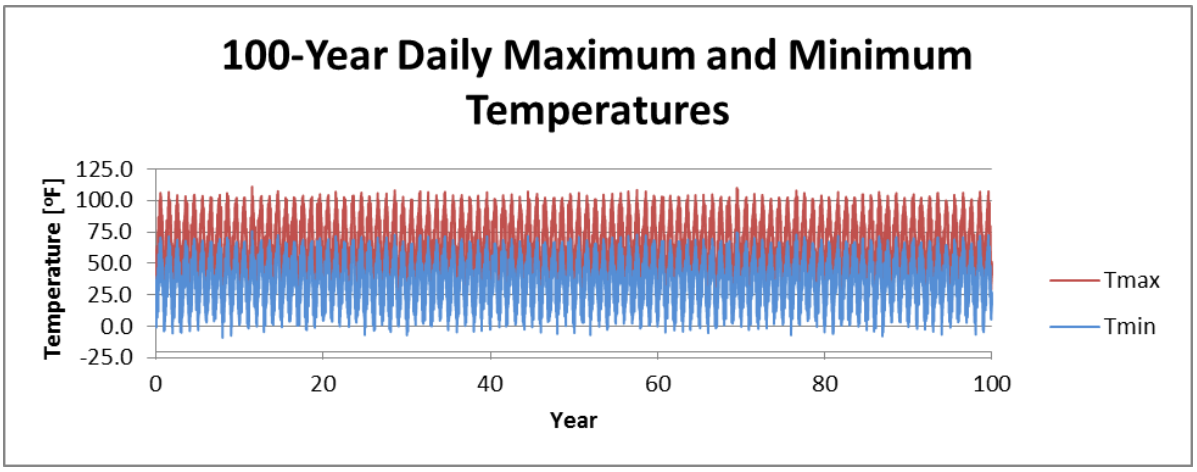

Figure 8. 100-year daily Tmax and Tmin record generated from a 30-year record available from the Dugway, Utah NOAA station.

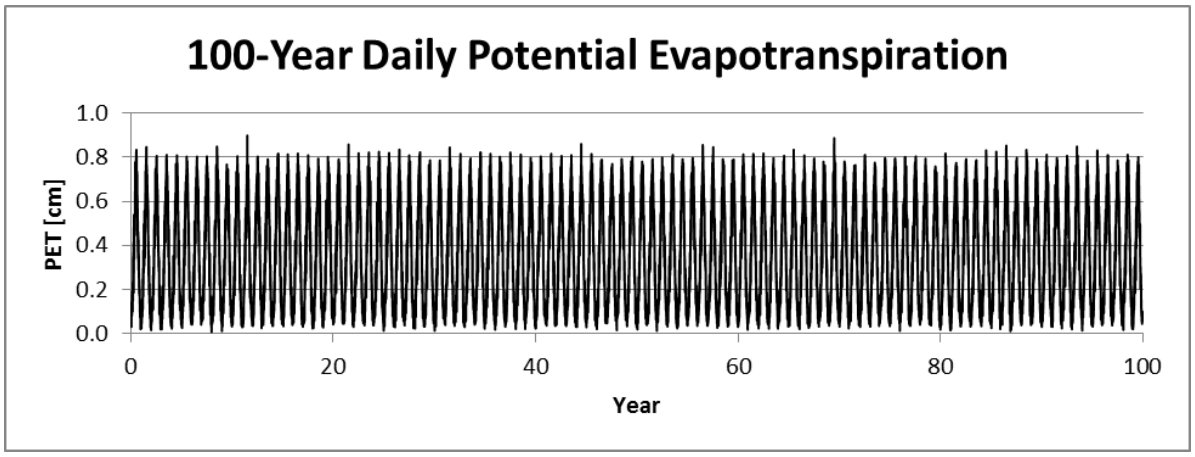

Figure 9. 100-year daily potential evaporation generated using the Hargreaves method.

Root water uptake depends on the estimation of daily potential transpiration (described above), the depth of the rooting zone, the variation of root density with depth, and the parameters used to describe the water stress function. Measurements of rooting depth and root distribution were made in two excavations by SWCA (2011). Rooting depths and density for the two most prevalent species are shown in Figure 10.

Root distribution was modeled as extending into the frost protection layer with a maximum depth of 31 inches (80 cm). Root density was modeled as decreasing linearly with depth.

The van Genuchten S-shaped model (van Genuchten, 1987) was used to model root water uptake. In this model the actual root water uptake is given by the potential transpiration multiplied by a water stress response function. For soil water pressures above the wilting point the water stress response function is given by

$$\alpha(h,h_\phi) = \frac{1}{1+\left(\frac{h+h_\phi}{h_{50}}\right)^p} \tag{37}$$

where h is the soil pressure head, h_φ is the osmotic head and h_{50} and p are parameters. Given the discussion in Section 6 on osmotic potential, the osmotic stress is assumed to be negligible for these simulations so h_φ is zero. The parameter h_{50} corresponds to the pressure head at which water uptake is reduced by 50 percent. A value of -200 cm was used for these simulations. A HYDRUS default value of 3 was used for the exponent p. The water stress response function with these parameters is shown in Figure 11.

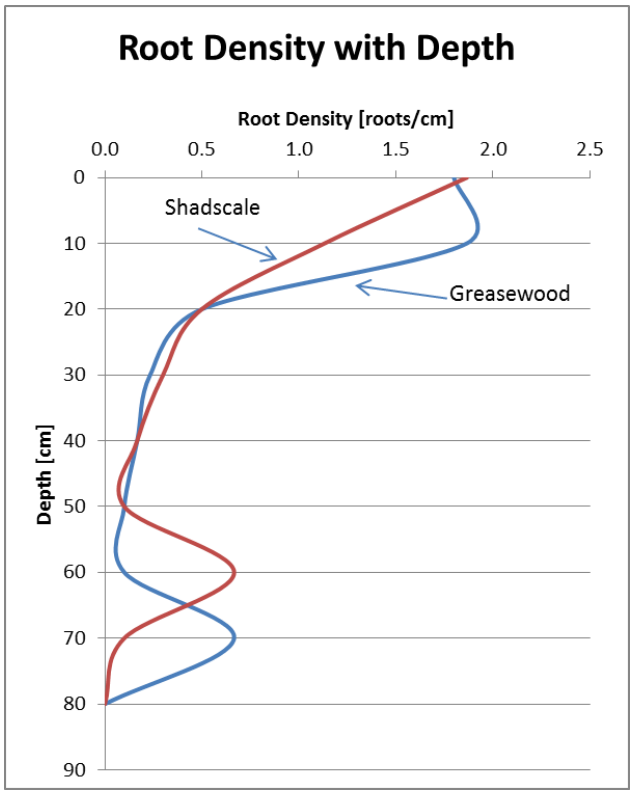

Figure 10. Root density with depth at the Clive Site for Shadscale and Black Greasewood [SWCA 2011].

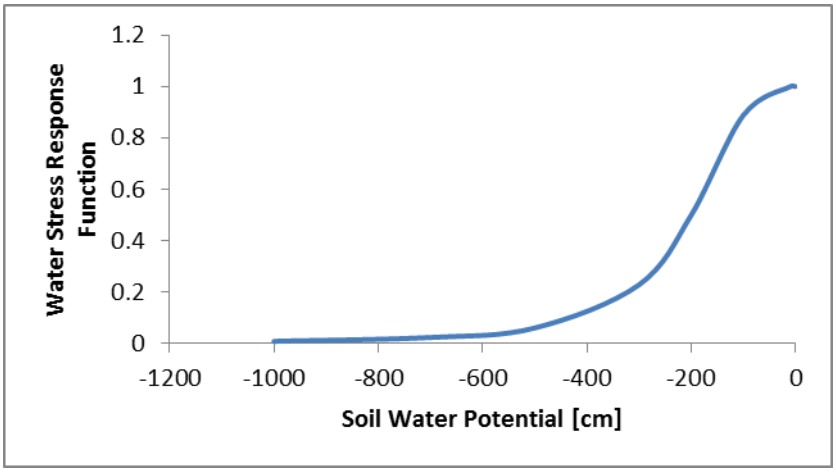

Figure 11. Water stress response function for root water uptake model.

12.4 Model Geometry

The HYDRUS-1D models were constructed using the maximum number of nodes (1001), with nodes evenly spaced down a 152-cm deep profile such that each node had a 0.152-cm spacing. The top slope of the waste cover was simulated, with a slope set to 2.4% (1.4 degrees).

The HYDRUS-1D model geometry for all simulations is shown in Figure 2, which shows the thickness of each material layer in the ET cover. Observation nodes were placed in the center of each layer, with an additional node at the bottom boundary.

12.5 Material Properties

The hydraulic properties for each of the layers within the ET cover for the HYDRUS-1D modeling are summarized in Table 8. The source of each hydraulic property for each layer is provided in this Table. Bingham (1991, p. B-20) is the source of hydraulic properties measured on core samples collected at the Clive site. Whetstone (2011, Table 17) is the source of the design specifications for the K_s of the two radon barriers. For the frost protection layer, hydraulic properties for a sandy loam were used and taken from the HYDRUS-1D pull-down menu which includes properties from the database of Carsel and Parrish (1988). Table 8 also identifies several properties as "Variable". These properties were associated with an infiltration and water content model based on statistical distributions of hydraulic properties developed to provide net infiltration and volumetric water content to the GoldSim DU PA Model.

The nine cores sampled from Unit 4 at the site and listed in Table 4 are all described as a silty clay texture. However, hydraulic properties were available for only two of the nine cores (see Appendix). To provide a better estimate of the uncertainty of the hydraulic properties of Unit 4 that compose the surface and evaporative zone layers of the ET cover, the α and n values were taken from the distributions (mean and standard deviation) for each parameter from the Rosetta database of hydraulic parameters for the textural class of silty clay (Schaap 2002). The standard deviations were converted to standard errors by dividing by √n where n is the number of samples, 28 in this case. The distributions for α and n are summarized here:

A: log (base-10) mean = -1.79, log (base-10) standard error = 0.1209

N: log (base-10) mean = 0.121, log (base-10) standard error = 0.0189

where $\alpha = 10^{A}$ and $n = 10^{N}$. The units of α are 1/cm and n is dimensionless.

Normal distributions of A and N were sampled 20 times, and then transposed from log space by calculating 10^{A}, and 10^{N} for the 20 sampled values. In addition, N was truncated such that it could not be less than 0.0 (required in Eqn. 32).

An expanded assessment of the performance of the radon barriers was made possible by developing a distribution for the saturated hydraulic conductivity (K_s) of the radon barriers to use for the modeling. The K_s values for the radon barriers were sampled from a distribution developed from a minimum value of 4×10^{-3} cm/day corresponding to the design specification for the upper radon barrier (Whetstone 2007, Table 8), and 50^{th} and 99^{th} percentile values of 0.7

cm/day and 52 cm/day, respectively, which are from a range of in-service ("naturalized") clay barrier K_s values described by Benson et al. (2011, Section 6.4, p. 6-12). A normal distribution was fit to the 50th and 99th percentiles, and the minimum value of 4E-3 cm/day was used as a shift. For all HYDRUS simulations, the same K_s value was applied to both the upper and lower radon barriers.

Correlations between α and n were investigated by analyzing the combinations of α and n for the 12 textural classes in Rosetta (Schaap, 2002), and no correlations were evident. There were also no correlations between K_s and α or n.

The developed 20 sets of uncertain parameters for α, n, and K_s were then used as hydraulic property inputs to 20 1000 year simulations using HYDRUS-1D.

Twenty HYDRUS-1D simulations were conducted to evaluate the uncertainty in infiltration flux into the waste zone, and water content within each ET cover layer as a function of hydraulic property uncertainty. While it is preferable to sample distributions of uncertain hydraulic parameters for all waste layers, a modified approach was used where van Genuchten (1980) α and n parameters for the surface and evaporative zone layers, and the K_s of the radon barriers were randomly sampled from distributions for each, to generate 20 parameter sets of α, n, and K_s. These 20 parameters sets are shown in Table 9.

Table 8. Hydraulic properties of topslope cover used for HYDRUS modeling.

Layer	Parameter	Value	Units	Source	Notes
Surface	θ_r	0.111	[-]	Rosetta database for Silty clay	
	θ_s	0.4089	[-]	Rosetta database for Silty clay	Adjusted for 15% gravel
	α	*Variable*	1/cm	Rosetta database	See Table 9.
	n	*Variable*	[-]	Rosetta database	See Table 9.
	K_s	4.46	cm/day	Table 1, Unit 4 Properties	
Evaporative Zone	θ_r	0.111	[-]	Rosetta database for Silty clay	
	θ_s	0.481	[-]	Rosetta database for Silty clay	
	α	*Variable*	1/cm	Rosetta database	See Table 9.
	n	*Variable*	[-]	Rosetta database	See Table 9.
	K_s	4.46	cm/day	Table 1, Unit 4 Properties	
Frost Protection	θ_r	0.065	[-]	Carsel and Parrish (1988)	Šimůnek and Šejna (2011), Table 7, Sandy Loam
	θ_s	0.41	[-]	"	"
	α	0.075	1/cm	"	"
	n	1.89	[-]	"	"
	K_s	106.1	cm/day	"	"
Upper Radon Barrier	θ_r	0.1	[-]	Whetstone (2011) Table 17, p. 25	Compacted Unit 4 borrow soils
	θ_s	0.432	[-]	"	"
	α	0.003	1/cm	"	"
	n	1.172	[-]	"	"
	K_s	*Variable*	cm/day	Whetstone (2011) Table 17, p. 25; Benson et al., (2011)	See Table 9.
Lower Radon Barrier	θ_r	0.1	[-]	Whetstone (2011) Table 17, p. 25	Compacted Unit 4 borrow soils

Layer	Parameter	Value	Units	Source	Notes
	θ_s	0.432	[-]	"	"
	α	0.003	1/cm	"	"
	n	1.172	[-]	"	"
	K_s	*Variable*	cm/day	Whetstone (2011) Table 17, p. 25; Benson et al., (2011)	See Table 9.

Table 9. Parameter sets of van Genuchten α and n, and K_s used for HYDRUS modeling.

Replicate	α (1/cm)	n	K_s (cm/d)
1	0.005221	1.634226	1.421036
2	0.008384	1.438333	0.953734
3	0.002048	1.343555	2.864782
4	0.028901	1.038489	0.622561
5	0.04857	1.028887	1.949663
6	0.001883	1.085208	0.555409
7	0.015117	1.38004	10.20695
8	0.004667	1.10274	1.86598
9	0.009796	1.837374	1.280137
10	0.009963	1.310235	2.354076
11	0.05807	1.882767	3.3506
12	0.043011	1.390255	2.211774
13	0.013965	1.193309	1.357634
14	0.037984	1.349198	0.593308
15	0.032913	1.193675	0.177924
16	0.021098	1.713354	7.260783
17	0.048946	1.06616	0.461682
18	0.004078	1.466295	3.482155
19	0.043043	1.151677	2.398727
20	0.3021	1.255238	0.161262

12.6 Boundary Conditions

The atmospheric boundary condition in HYDRUS provides the top boundary of the model with daily values of precipitation, potential evaporation, and potential transpiration at the soil-air interface. A free drainage boundary condition is applied at the bottom of the model as a unit gradient boundary condition where the water flux across the boundary is equal to the flux due to gravity at the water content of the material. HYDRUS calculates and reports surface runoff, evaporation, and infiltration fluxes for the atmospheric boundary and fluxes for the free drainage boundary.

12.7 Initial Conditions

An initial pressure head condition of -200 cm was applied to the entire model domain. This pressure head corresponds to a slightly unsaturated condition for the fine-grained materials. The model is deliberately run for a long period of time (1,000 years) in order reach a near-steady state net infiltration rate that is not influenced by the initial conditions.

12.8 Cases Simulated

As discussed above, 20 HYDRUS-1D simulations were conducted to evaluate the uncertainty in infiltration flux into the waste zone, and water content within each ET cover layer as a function of hydraulic property uncertainty. The twenty simulations are named Rep1 through Rep20, with varying van Genuchten α and n, and K_s values shown in Table 9.

Simulations were run for 1,000 years. The mean of the fluxes into the top of the waste layer and the mean water contents for the surface layer, evaporative zone, frost protection layer, upper and lower radon barriers over years 900 to 1000 were calculated.

12.9 Model Results

The 20 HYDRUS-1D simulations resulted in a distribution of average annual infiltration into the waste zone, and average volumetric water contents for each ET cover layer. Infiltration flux into the waste zone ranged from 0.007 to 2.9 mm/yr, with an average of 0.42 mm/yr, and a log mean of 0.076 mm/yr for the 20 replicates.

Multiple linear regression models were fit to the HYDRUS infiltration results, and water contents for each ET cover layer. The general form of the regression was:

$$Y = \beta_0 + \beta_1 * K_S + \beta_2 * \alpha + \beta_3 * n \quad (38)$$

Net infiltration is in units of mm/yr and volumetric water content is dimensionless. For the net infiltration flux regressions, K_s was dropped as a predictor due to poor fit of the models. The regressions were fit using the 'lm()' function in the software package R, which uses least squares for estimating parameters. All values of β coefficients are summarized in Table 10.

Table 10. Coefficients calculated from multiple linear regression models.

Coefficient	β_o	β_1	β_2	β_3
SurfaceWC	0.554	-0.00197	-0.0555	-0.222
EvapWC	0.684	-0.00222	-0.157	-0.288
FrostWC	0.0726	0.000169	0.0521	-7.27E-06
Rn1WC	0.3	-0.00361	0.314	-0.013
Rn2WC	0.3	-0.00361	0.314	-0.013
Flux (mm/yr)	0.959	N/A	4.4	-0.521

13.0 Implementation in GoldSim

Average annual infiltration flux into the waste zone, and the volumetric water content of each ET cover layer was calculated using Equations 39 and 40, developed from HYDRUS-1D simulation results. GoldSim calculates values using Equations 39 and 40 for each ET cover layer.

The resulting equations for solving infiltration and water content in GoldSim become:

$$Infil = \beta_0 + \beta_2 * \alpha + \beta_3 * n \quad (39)$$

$$WC = \beta_{i,0} + \beta_{i,1} * K_S + \beta_{i,2} * \alpha + \beta_{i,3} * n \quad (40)$$

where *Infil* is net infiltration in mm/yr, *WC* is average volumetric water content, and β values are linear regression coefficients with the subscript *i* corresponding to Surface, Evaporative zone, Frost protection, Upper radon barrier, and Lower radon barrier layers. The necessary distributions in GoldSim are VG_logAlpha, VG_logN, and RnBarrierKsat_Natdist.

α and n are calculated from values drawn from distributions using:

$\alpha = 10^{\text{VG\_logAlpha}}, where\ \text{VG\_logAlpha} \sim Normal(mean: -1.79, se: 0.1209)$ and

$n = 10^{\text{VG}_{\text{logN}}}, where\ \text{VG}_{\text{logN}} \sim Normal(mean: 0.121, se: 0.0189)$.

K_s is sampled using:

$\text{RnBarrierKsat\_Natdist} = K_s, \sim Lognormal(geom.mean: 0.691, geom.sd: 6.396)$, with right shift of 0.00432.

Volumetric water contents for the waste, clay liner and native Unit 3 soil below the Federal DU cell at the Energy*Solutions* Clive Facility are calculated using a numerical method. The development and testing of this method implemented in the GoldSim DU PA model are described in the Appendix.

14.0 Sensitivity Analysis: Additional HYDRUS-1D Simulations

Results from the 20 replicate HYDRUS-1D simulations were used to calculate the regression equations for *Infil* and *WC* that were implemented in GoldSim. However, additional HYDRUS-1D simulations were conducted to specifically investigate the sensitivity of net infiltration to the K_s of the radon barrier and rooting depth. Results of these additional model runs were not carried forward and not implemented directly in GoldSim. However, the distribution for the K_s of the radon barriers in the Clive DU PA model as described above in Section 12.5 is based on the range of K_s used for these simulations.

For these additional model runs, nine simulations were conducted with three values of K_s and three values of rooting depth. The low K_s simulations used the as-built K_s values (0.00432 and 0.0864 cm/day for upper and lower radon barriers, respectively) while the medium and high K_s simulations used the same valued described above from Benson et al. (2011): 0.691 and 51.8 cm/day (one value used for both upper and lower radon barriers). Three values of maximum rooting depth were also simulated: 40, 80, and 120 cm. Unlike the 20 replicate simulations described above and whose results were implemented in GoldSim, these simulations used hydraulic properties for the Surface and Evaporative layers for Unit 4 borrow soils reported in Bingham (1991, p. B-20, sample GW19A-B1).

Results of these sensitivity model runs are shown in Table 11 where it is apparent that infiltration is insensitive to the K_s of the radon barrier, and even less sensitive to rooting depth. This lack of sensitivity can be explained by the remarkable hydraulic properties of the Surface layer and Evaporative layer that are both comprised of Unit 4 soil, a material that performs well as a storage and release (by evaporation) material. It is notable that the texture the Unit 4 soil is considerably more clayey and silty than the silty clay properties from Schaap (2002) that were used for the 20 replicates.

Table 11. Results of HYDRUS-1D Sensitivity Analysis Simulations.

Infiltration into waste zone (mm/year)				
		Maximum Rooting Depth (cm)		
		40	80	120
Upper Rn Barrier Ksat (cm/d) Lower Rn Barrier Ksat (cm/d)	0.00432 0.0864	0.0098	0.0097	0.0097
Upper Rn Barrier Ksat (cm/d) Lower Rn Barrier Ksat (cm/d)	0.691 0.691	0.0082	0.0082	0.0082
Upper Rn Barrier Ksat (cm/d) Lower Rn Barrier Ksat (cm/d)	51.8 51.8	0.0055	0.0055	0.0055

15.0 Contaminant Fate and Transport in Porous Media

Once all the hydraulic properties and states have been developed, as in the previous sections, we can turn to transport mechanisms within the various porous media. Contaminant transport takes place in fluid phases—in the present case, this is limited to air and water. Fluids move through the pores by advection in response to fluid pressure gradients, carrying dissolved contaminants with them. Fluids are also a medium for diffusive transport, in which contaminants move simply in response to concentration gradients, and do not require movement of the fluid. Both these processes occur simultaneously, along with all the other mechanisms identified in the model for contaminant transport (radioactive decay and ingrowth, geochemical partitioning, biotically induced transport, erosion, etc.) This section discusses advective and diffusive contaminant transport mechanisms in fluids.

15.1 Porous Medium Water Transport

Water is a transport pathway considered at Clive, and the conceptual model includes the advection of solutes in water moving down from the waste to the shallow aquifer as well as diffusion of solutes in pore water.

15.1.1 Advection of Water

The flow of water is discussed at length in the previous sections of this document. Contaminant transport in this flowing water is essentially passive, with solutes moving along with the fluid, though of course concentrations are affected by other simultaneous processes.

15.1.2 Diffusion in Water

The Clive DU PA Model employs a modified version of GoldSim's native diffusive flux links to calculate diffusive fluxes in porous media. The modifications are necessary to account for unsaturated media, since GoldSim assumes that porous media are saturated in its basic implementation of diffusive flux calculations. The standard GoldSim diffusive flux mathematics are covered in Appendix B of the GoldSim User's Guide (GTG, 2011), and the modifications

that have been developed by Neptune are discussed in detail in the Neptune document entitled Modeling Diffusion in GoldSim, but are also covered briefly here. The modifications required to model diffusion in unsaturated media take two phenomena into consideration: 1) The diffusive area is reduced by the saturation (with respect to air or water, whichever medium is of interest) and 2) the diffusive length is increased to account for tortuosity in the respective medium.

If a porous medium contains only a single fluid phase, the diffusive area between two cells containing that medium is simply the total area times the porosity, since the pores are occupied by the fluid, and the diffusion takes place only in the fluid. In the case of two fluids, such as air and water in unsaturated media, the diffusive area is further reduced, since the area of the fluid of interest across the plane of diffusion is less. If we are interested in diffusion in the water phase, for example, the area of water that intersects the plane is equal to the total area times the water content, which equals the total area times the porosity times the saturation with respect to water. If we are interested in diffusion in the air phase, we use the same construct, substituting air for water. Because the diffusive area is always less, the diffusion in a unsaturated medium will always be less than that in a fully saturated medium.

Diffusion in unsaturated media is also attenuated because of increased tortuosity. In any porous medium, a diffusing solute must travel through pores, following a tortuous path that is always longer than if it were traveling in a straight line. The ratio of the straight line distance to this tortuous path is called the tortuosity. If the porous medium is unsaturated, this path becomes even longer, since the three dimensional shape of the fluid of interest gets even more tortuous. This increases the diffusive length, which is used in calculating the concentration gradient. The gradient in concentration of a solute is what drives diffusion.

15.1.3 Water Phase Tortuosity

Tortuosity is a term used to describe the resistive and retarding influence of pore structure for a variety of transport processes (Clennell, 1997). Definitions of tortuosity are not consistent in the literature and depend on the discipline and the particular transport process of interest. The tortuosity τ for molecular diffusion in porous media can be written as the ratio of effective diffusivity D_{eff} to bulk diffusivity D_{bulk}, often seen in two forms:

$$\tau_1 = \frac{D_{eff}}{D_{bulk}} \tag{41}$$

or alternatively, if the measured porosity n is explicit (Clennell, 1997), as

$$\tau_1 = \frac{D_{eff}}{n\, D_{bulk}} \tag{42}$$

In this definition, consistent with the assumptions of GoldSim's internal calculations, the value of tortuosity varies between 0 and 1, with lower values indicating a longer path for porous medium solute transport via diffusion.

For unsaturated systems, n is replaced in equation (42) by water content θ_w for water phase diffusion, or by the volumetric air content θ_a, for gaseous phase diffusion. The form shown in

equation (41) is found in Freeze and Cherry (1979) and Marsily (1986) while that in equation (42) is used by Hillel (1980) and Koorevaar et al. (1983).

For consistency with GoldSim the second form is used. The equations for diffusive transport in GoldSim explicitly specify the effective porosity (or in the case of unsaturated flow, water content or air filled porosity) as in equation (42). For more information on the diffusive mass flux equations in GoldSim, see Appendix B of the GoldSim User's Guide (GTG, 2011). In the following sections, the equations from the literature have been converted where necessary to be consistent with equation (42) so that they can be directly applied to GoldSim models.

Two options were considered for modeling liquid phase tortuosity in the models. The Millington-Quirk model is commonly used to estimate tortuosity in non-fractured porous media (Millington and Quirk, 1961) (see Jury and Horton, 2004, eq. 7.14, modified by division by water content for consistency with GoldSim.) The water phase tortuosity τ_w is calculated as

$$\tau_w = \frac{D_{eff}}{\theta_w \, D_{bulk}} = \frac{\theta_w^{7/3}}{n^2} \tag{43}$$

Water phase tortuosity will be implemented in the Clive DU PA model using the form shown in equation (42). The exponents will be treated as distributions in order to allow the sensitivity analysis to determine if the model is sensitive to the values of the exponents. The water content exponent is described by a normal distribution with a mean of 7/3 and a standard deviation of 0.01 and the porosity exponent is described by a normal distribution with a mean of 2 and a standard deviation of 0.01.

15.2 Porous Medium Air Transport

15.2.1 Advection of Air

Air-phase advection is not included in the Clive DU PA Model. It is assumed that the advective flux of gases is negligible compared to the diffusive gas flux.

15.2.2 Diffusion in Air

Air-phase diffusion is included in the model, and this is the principal process by which gases are moved. The “built-in” diffusion calculations in GoldSim are used to estimate diffusion in the air phase. These gaseous diffusive fluxes are modified to handle the unsaturated porous media (described above in Section 14.1.2), but also include a calibration to counteract numerical dispersion for radon (discussed in the Radon Transport white paper), which at this time is the only radionuclide that is considered to be present in the gaseous phase.

Diffusion in the air phase is modeled throughout the top slope column, bounded at the bottom by the saturated zone, and at the top by the atmosphere. The bottom boundary condition is one of no diffusion, since there is no air in the saturated zone to diffuse into, by definition. The boundary condition at the top is effectively a zero-concentration sink, since the volume of air in the atmosphere flowing over the embankment is sufficiently large that concentrations are kept much lower than in the pore air of the cover and wastes below. In order to model this, the air directly

above the embankment is represented by an Atmosphere Cell Pathway element in GoldSim. The volume of air is defined by a thickness times the area of each respective modeled column, and this air volume is flushed out by the wind. The diffusive flux from the uppermost cover cell in the column to the Atmosphere cell is defined by the diffusive area, as discussed above, and the diffusive length, discussed in the following section. Since the atmosphere is not a porous medium, a diffusive length unrelated to its thickness is adopted. Since the wind will maintain low concentrations in the atmosphere, amounting to a zero-concentration boundary condition, the choice of the parameters defining the Atmosphere is not expected to have much influence on the diffusive flux from the embankment cover. Small uncertainties have been selected for these values, as shown in Table 12, in order to evaluate the model's sensitivity.

Table 12. Atmosphere volume parameters for creating a surface boundary condition in the porous medium air diffusion model.

Parameter	Distribution	Units
Thickness of the atmosphere layer	N(μ=2.0, σ=0.5, min=Small, max=Large)	m
Wind speed	N(μ=3.14, σ=0.5, min=Small, max=Large)	m/s
Atmospheric diffusion length	N(μ=0.1, σ=0.02, min=Small, max=Large)	m

15.2.3 Air-Phase Tortuosity

A number of tortuosity models have been proposed for air phase diffusion in porous media. Using the form for tortuosity shown in (42) above, models reviewed by Jin and Jury (1996) include the Penman model (Penman, 1940) and two models attributed to Millington and Quirk. In the Penman model, air phase tortuosity τ_a is a constant:

$$\tau_a = 0.66. \tag{44}$$

In the more commonly used Millington-Quirk model (MQ1), which is analogous to equation (43), tortuosity is expressed as

$$\tau_a = \frac{\theta_a^{7/3}}{n^2} \tag{45}$$

And, in an alternative Millington-Quirk model (MQ2) evaluated by Jin and Jury (1996), tortuosity is expressed as

$$\tau_a = \frac{\theta_a}{n^{2/3}} \tag{46}$$

Note that as θ_a approaches n (e.g. as the porous medium becomes drier), τ_a approaches $n^{1/3}$ for both formulations (45) and (46).

An air-phase tortuosity model was developed by Lahvis et al. (1999) by calibrating a transport model to steady-state gas concentration data obtained from seven column experiments using silt and fine sand sediments. In this model, air phase tortuosity is dependent only on the volumetric water content:

$$\tau_a = 0.765 - 2.02\theta_w \tag{47}$$

Comparison of these models for alluvium with an effective porosity of 0.37 and tortuosity as defined in equation (42) is shown in Figure 12. Due to the similarity of the Lahvis et al. (1999) model to the MQ2 model over a wide range of volumetric water content, it will not be considered further.

The Penman and the two Millington-Quirk models were compared by Jin and Jury (1996) with measured D_{eff} /D_{bulk} ratios from six studies that included a total of approximately 50 measurements on predominantly agricultural soils. While this ratio corresponds to the definition of tortuosity given in equation (42), it is useful in comparing the predictions of the various models. Over the range of air phase porosity investigated (0.05 to 0.5), the Penman model tended to overestimate tortuosity, while the MQ1 model in equation (45) underestimated tortuosity. Of the three models, the MQ2 model given by (46) provided the best fit to the measured tortuosities.

A comparison of the Penman and Millington-Quirk models for a material with an effective porosity of 0.37 is shown in Figures 12 and 13. Note that in both these figures, the points are merely points of calculation, and do not represent data. The values produced by the Penman and Millington-Quirk models converge for dry and wet conditions but diverge at intermediate values of air porosity. Given its median behavior as seen in Figures 12 and 13, the alternative Millington-Quirk model (MQ2, equation (46)) is used in the Clive DU PA model.

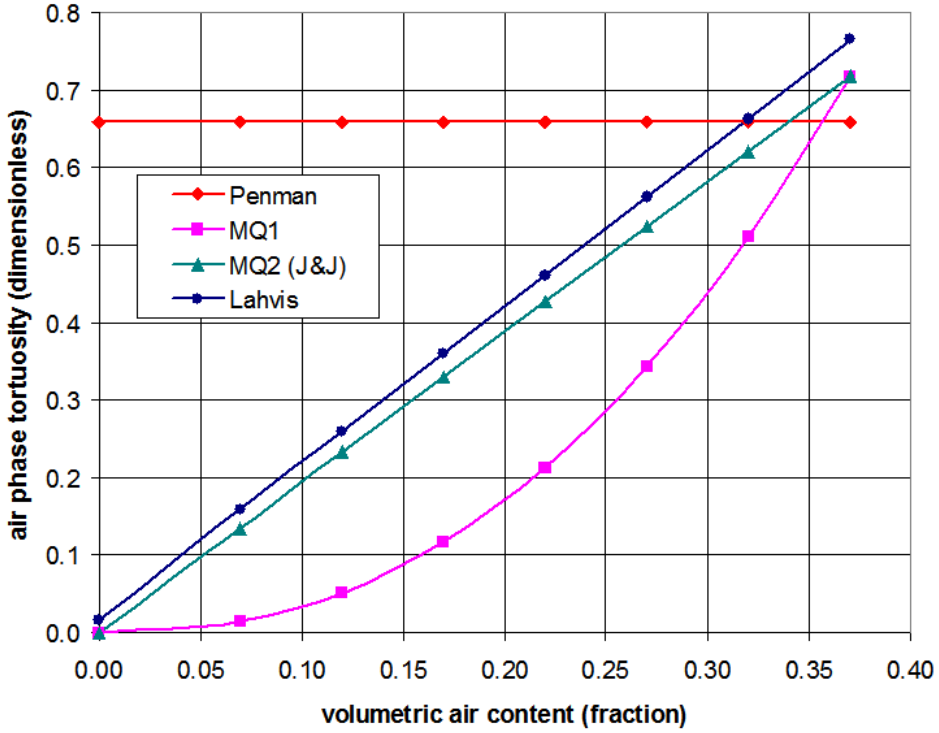

Figure 12. Comparison of air-phase tortuosity models by Penman (equation (44)), Millington and Quirk (MQ1, equation (45)), Millington and Quirk as modified by Jin and Jury (1996) (MQ2, equation (46)), and Lahvis et al. (1999) (equation (47)).

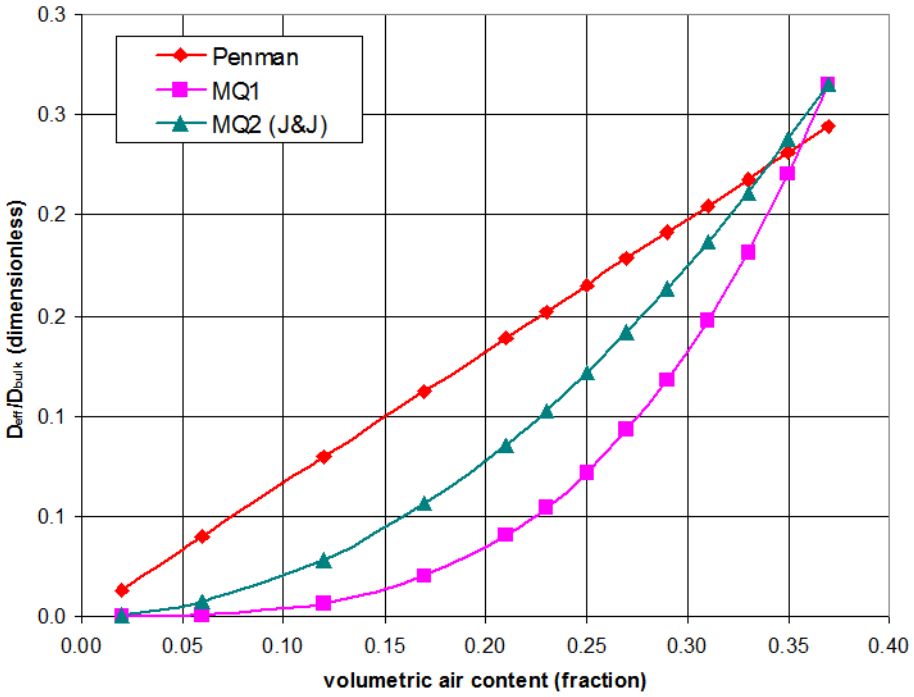

Figure 13. Comparison of effective to bulk diffusivity ratios with air phase porosity for air phase tortuosity models.

Tortuosity is implemented in the GoldSim model as a multiplier to the diffusive length, which is defined for each Cell Pathway element using the common method of setting it equal to 1/2 the cell length that is parallel to flow. In this case, that is the vertical dimension.

16.0 References

Anderson, Michelle D. 2004. *Sarcobatus vermiculatus. In: Fire Effects Information System, [Online]*. U.S. Department of Agriculture, Forest Service, Rocky Mountain Research Station, Fire Sciences Laboratory (Producer). Available from: http://www.fs.fed.us/database/feis/ [2013, November 7].

Benson, C.H., W.H. Albright, D.O. Fratta, J.M. Tinjum, E. Kucukkirca, S. H. Lee, J. Scalia, P. D. Schlicht, and X. Wang. 2011. *Engineered Covers for Waste Containment: Changes in Engineering Properties & Implications for Long-Term Performance Assessment*, NUREG/CR-7028, Office of Research, U.S. Nuclear Regulatory Commission, Washington, DC.

Bingham Environmental. 1991. *Hydrogeologic report Envirocare Waste Disposal Facility South Clive, Utah.* October 9, 1991. Prepared for Envirocare of Utah. Salt Lake City, UT.

Bingham Environmental. 1994. *Hydrogeologic report Mixed Waste Disposal Area Envirocare Waste Disposal Facility South Clive, Utah.* November 18, 1994. Prepared for Envirocare of Utah. Salt Lake City, UT.

Black, B.D., B.J. Solomon, and K.M. Harty, 1999. *Geology and geologic hazards of Tooele Valley and the West Desert Hazardous Industry Area, Tooele Count, Utah*, Special Study 96, Utah Geological Survey, Salt Lake City, Utah.

Carsel, R. F., and R. S. Parrish. 1988. *Developing joint probability distributions of soil water retention characteristics.* Water Resources Research, 24(5):755-770, 1988.

Clennell, M.B. 1997. *Tortuosity: a guide through the maze*. in Developments in Petrophysics, Lovell, M.A. and P.K. Harvey (eds). Geological Society Special Publication No. 122, pp. 299-344.

CRC. 1985. CRC Handbook of Chemistry and Physics, 66th Edition. R.C. Weast, M.J. Astle, and W.H. Beyer (eds.). *Osmotic parameters and electrical conductivities of aqueous solutions.* p. D-269. CRC Press Inc. Boca Raton, FL.

Diodato, D.M., 2000. *Review: HYDRUS-2D*, Ground Water 38:10–11.

Energy*Solutions*, 2012, *Utah Low-Level Radioactive Material License (RML UT2300249) Updated Site-Specific Performance Assessment*, October 8, 2012, Energy*Solutions*, LLC, Salt Lake City, UT

Envirocare of Utah, Inc. 2000. Revised hydrogeologic report for the Envirocare Waste Disposal Facility Clive, Utah. Version 1.0. Envirocare of Utah, Inc. Salt Lake City, UT.

Envirocare of Utah, Inc. 2004. Revised hydrogeologic report for the Envirocare Waste Disposal Facility Clive, Utah. Version 2.0. Envirocare of Utah, Inc. Salt Lake City, UT.

Fayer, M.J., 2000. *UNSAT-H Version 3.0: Unsaturated Soil Water and Heat Flow Model, Theory, User Manual, and Examples*. PNNL-13249. Pacific Northwest National Laboratory, Richland, Washington. June, 2000.

Freeze, R.A and J.A. Cherry. 1979. *Groundwater*. Prentice-Hall, Inc., Englewood Cliffs, NJ.

Gates, J.S. and S.A. Kruer, 1981. *Hydrologic reconnaissance of the Southern Great Salt Lake Desert and summary of the hydrology of West-Central Utah*, State of Utah Department of Natural Resources, Technical Publication No. 71, Salt Lake City, UT.

GTG (GoldSim Technology Group), 2011. *User's Guide: GoldSim Contaminant Transport Module*, GoldSim Technology Group, Issaquah, WA, December 2010.

Goodman, P.J. 1973. *Physiological and Ecotypic Adaptations of Plants to Salt Desert Conditions in Utah.* Journal of Ecology, Vol. 61, No. 2, pp. 473-494.

Hillel, D. 1980. *Fundamentals of Soil Physics*. Academic Press Inc. San Francisco, CA.

Jin, Y., and W.A. Jury. 1996. *Characterizing the Dependence of Gas Diffusion Coefficient on Soil Properties*, Soil Science Society of America Journal, Vol. 60, pp. 66-71.

Jury, W.A. and R. Horton. 2004. *Soil Physics.* 6th ed. John Wiley and Sons Inc. New Jersey.

Koorevaar, P., G. Menelik, and C. Dirksen. 1983. *Elements of Soil Physics*. Elsevier. New York, NY.

Lahvis, M.A., A.L. Baehr, and R.J. Baker. 1999. *Quantification of Aerobic Biodegradation and Volatilization Rates of Gasoline Hydrocarbons Near the Water Table Under Natural Attenuation Conditions*. Water Resour. Res. v. 27, 753-765.

Marsily, G. de. 1986. *Quantitative Hydrogeology*. Academic Press Inc. San Diego, CA.

McCray, J., 2007. *HYDRUS: Software review*, Southwest Hydrol. 6(1):41.

Meteorological Solutions, 2012. *January 2011 Through December 2011 and January 1993 through December 2011 Summary Report of Meteorological Data Collected at EnergySolutions' Clive, Utah Facility*, Project No. 011110111, February 2012.

Millington, R.J., and J.P. Quirk. 1961. *Permeability of porous solids*. Trans. Faraday Society (57) pp. 1200-1207

Mualem, Y. 1976. *A New Model for Predicting the Hydraulic Conductivity of Unsaturated Porous Media*. Water Resources Research, Vol. 12, No. 3, pp. 513-522. June, 1976.

Neitsch, S.L., J.G. Arnold, J.R. Kinry, and J.R. Williams, 2005. *Soil and Water Assessment Tool Theoretical Documentation: Version 2005*, Grassland, Soil and Water Research Laboratory Agricultural Research Service and Blackland Research Center, Texas

Agricultural Experiment Station, Temple TX.
http://swatmodel.tamu.edu/media/1292/swat2005theory.pdf Accessed 7/24/2012.

NRCS. 2013. U.S. Department of Agriculture, Natural Resources Conservation Service. Web Soil Survey. Available from:
http://websoilsurvey.sc.egov.usda.gov/App/HomePage.htm
[Accessed 2013, November 7].

Pavek, Diane S. 1992. *Halogeton glomeratus. In: Fire Effects Information System, [Online]*. U.S. Department of Agriculture, Forest Service, Rocky Mountain Research Station, Fire Sciences Laboratory (Producer). Available from:
http://www.fs.fed.us/database/feis/

Penman, H.L. 1940. *Gas and vapor movements in the soil. I. The diffusion of vapors through porous solids*. Journal of Agricultural Science (30) pp. 437-462.

Richardson, C.W. and D.A. Wright, 1984, *WGEN: A Model for Generating Daily Weather Variables.* U. S. Dept. of Agriculture, Agricultural Research Service, ARS-8.

Scanlon, B. 2004. *Review of Hydrus-1D,* Southwest Hydrology, 3(4):37.

Schaap, M. 2002. *Rosetta: A computer program for estimating soil hydraulic parameters with hierarchical pedotransfer functions.* Available from:
http://ag.arizona.edu/research/rosetta/download/rosetta.pdf

Schroeder, P.R., N.M. Aziz, C.M. Lloyd, and P.A. Zappi. 1994a. *The Hydrological Evaluation of Landfill Performance (HELP) Model: User's Guide for Version 3.* EPA/600/R-94/168a. U.S. Environmental Protection Agency Office of Research and Development. Washington, D.C.

Schroeder, P.R., T.S. Dozier, P.A. Zappi, B.M. McEnroe, J.W. Sjostrom, and R.L. Peyton. 1994b. *The Hydrological Evaluation of Landfill Performance (HELP) Model: Engineering Documentation for Version 3.* EPA/600/R-94/168b. U.S. Environmental Protection Agency Office of Research and Development. Washington, D.C.

Shabala, S. 2013. *Learning from halophytes: physiological basis and strategies to improve abiotic stress tolerance in crops.* Ann. Bot. doi: 10.1093/aob/mct205. Available from: http://aob.oxfordjournals.org/content/early/2013/09/30/aob.mct205.full [2013, November 7].

Simonin, Kevin A. 2001. *Atriplex confertifolia. In: Fire Effects Information System, [Online]*. U.S. Department of Agriculture, Forest Service, Rocky Mountain Research Station, Fire Sciences Laboratory (Producer). Available from:
http://www.fs.fed.us/database/feis/ [2013, November 7].

Šimůnek, J., M. Šejna, H. Saito, M. Sakai, and M. Th. van Genuchten, 2009, *The HYDRUS-1D Software Package for Simulating the One-Dimensional Movement of Water, Heat, and*

Multiple Solutes in Variably-Saturated Media, Department of Environmental Sciences, University of California Riverside, Riverside, CA.

Šimůnek, J. and M. Šejna. 2011. *Software Package for Simulating the Two- and Three-Dimensional Movement of Water, Heat and Multiple Solutes in Variably-Saturated Media: User Manual Version 2*, PC-Progress, Prague, Czech Republic.

SWCA. 2011. *Field Sampling of Biotic Turbation of Soils at the Clive Site, Tooele County, Utah*, January, 2011, SWCA Environmental Consultants, Salt Lake City, UT.

Utah Division of Water Rights, (DWR), water rights and well log database at http://waterrights.utah.gov/wrinfo/query.asp. Accessed March 18, 2014.

van Genuchten, M.Th. 1980. *A closed-form equation for predicting the hydraulic conductivity of unsaturated soils.* Soil Science Society of America Journal 44 (5): 892–898.

van Genuchten, M. Th. 1987. *A numerical model for water and solute movement in and below the root zone.* Research Report No 121, U.S. Salinity laboratory, USDA, ARS, Riverside, California, 1987.

Varado, N., I Braud, and P.J. Ross, 2005. *Development and assessment of an efficient vadose zone module solving the 1D Richards' equation including root extraction by plants*, Journal of Hydrology, 323, 258-275.

Wang, T., V. A. Zlotnik, J. Šimunek, and M. G. Schaap, 2009. *Using pedotransfer functions in vadose zone models for estimating groundwater recharge in semiarid regions*, Water Resour. Res., 45, W04412, doi:10.1029/2008WR006903.

Western Regional Climate Center, 2012. Dugway, Utah, 30 year daily temperature and precipitation summary. http://www.wrcc.dri.edu/cgi-bin/cliMAIN.pl?ut2257.

Whetstone Associates, Inc., 2011. *EnergySolutions Class A West Disposal Cell Infiltration and Transport Modeling Report*, dated November 28, 2011. Document Number 4104K111128.

Whetstone Associates, Inc., 2007. *EnergySolutions Class A South Cell Infiltration and Transport Modeling*. December 7, 2007.

Appendix A

Soil Moisture Data for Units 3 and 4

The data for soil moisture characteristics in Unit 3, a silty sand, and in Unit 4, a silty clay, are reproduced in the following tables, and are based on testing performed by Colorado State University (Bingham Environmental 1991, Appendix B, pages B 20 and B 26). Cores GW18 B4 and GW17A B5 are from Unit 3, and cores GW19A B1 and GW17A B2 are from Unit 4. Bulk density is defined in the units of g/cm3. Conductivity data have units of cm/s.

	GW18-B4		GW19A-B1		GW17A-B5		GW17A-B2	
	WATER CONTENT	MATRIC PRESSURE (cm)	WATER CONTENT	MATRIC PRESSURE (cm)	WATER CONTENT	MATRIC PRESSURE (cm)	WATER CONTENT	MATRIC PRESSURE (cm)
DRYING CYCLE	0.409	0	0.442	0	0.377	0	0.505	0
	0.409	6	0.438	383	0.376	19	0.505	49
	0.404	24	0.428	468	0.319	60	0.485	455
	0.362	94	0.405	683	0.207	274	0.466	954
	0.321	131	0.370	1074	0.188	569	0.453	1947
	0.262	171	0.344	2029			0.429	2563
	0.213	230	0.337	3025			0.397	4815
	0.180	349	0.316	4921				
	0.144	664						
	0.132	828						
WETTING CYCLE	0.117	932	0.316	4211	0.1279	946	0.395	4030
	0.119	852	0.317	3961	0.128	807	0.396	3537
	0.122	817	0.317	3736	0.128	578	0.399	3092
	0.126	683	0.322	3465	0.130	403	0.403	2545
	0.129	633	0.323	3265	0.134	282	0.407	2045
	0.135	491	0.327	3010	0.148	204	0.410	1524
	0.142	417	0.332	2774	0.186	88	0.413	1005
	0.156	314	0.335	2540	0.254	53	0.417	504
	0.171	262	0.343	2284	0.307	49	0.422	211
	0.180	221	0.345	2054	0.316	34	0.426	60
	0.220	110	0.352	1804				
	0.302	36	0.357	1534				
	0.327	9	0.365	1300				
			0.369	1079				
			0.373	845				
			0.383	625				
			0.398	391				
			0.397	300				
			0.432	0				
BULK DENSITY	1.567		1.397		1.673		1.326	
POROSITY	0.409		0.473		0.320		0.505	
WETTING CYCLE FIT PARAMETERS								
θ_s	0.380		0.432		0.345		0.429	
θ_s	0.0		0.0		0.130		0.172	
α	0.05222		0.00295		0.0177		0.0012	
n	1.3068		1.1202		3.6477		1.1000	
m	0.2347		0.1073		0.7259		0.0909	

	GW18-B4		GW19A-B1		GW17A-B5	
	WATER CONTENT	D(θ) (cm^2/s)	WATER CONTENT	D(θ) (cm^2/s)	WATER CONTENT	D(θ) (cm^2/s)
DIFFUSIVITY DATA	0.380	0.005559	0.430	0.004502	0.345	0.005559
	0.360	0.010385	0.420	0.004024	0.340	0.012307
	0.340	0.008981	0.400	0.003327	0.320	0.008794
	0.320	0.008246	0.380	0.002838	0.300	0.007767
	0.300	0.007759	0.360	0.002471	0.280	0.007184
	0.280	0.007401	0.340	0.002184	0.260	0.006785
	0.260	0.007119	0.320	0.001952	0.240	0.006485
	0.240	0.006889	0.315	0.001900	0.220	0.006247
	0.220	0.006696	0.312	0.001870	0.200	0.006051
	0.200	0.006529	0.262	0.001468	0.180	0.005885
	0.180	0.006383	0.212	0.001186	0.160	0.005742
	0.160	0.006254	0.162	0.000974	0.140	0.005616
	0.140	0.006138	0.112	0.000809	0.135	0.005586
	0.120	0.006034			0.132	0.005569
	0.100	0.005938			0.1308	0.005563
	0.080	0.005850			0.1305	0.005561
	0.060	0.005770				
	0.040	0.005695				
	0.020	0.005625				
	0.010	0.005591				
CONDUCTIVITY DATA	0.380	3.38E-5	0.430	1.89E-7	0.345	5.59E-5
	0.360	3.28E-5	0.420	1.33E-7	0.340	9.60E-6
	0.340	2.42E-5	0.400	6.74E-8	0.320	1.72E-5
	0.320	1.74E-5	0.380	3.41E-8	0.300	1.76E-5
	0.300	1.22E-5	0.360	1.71E-8	0.280	1.55E-5
	0.280	8.39E-6	0.340	8.38E-9	0.260	1.25E-5
	0.260	5.59E-6	0.320	4.01E-9	0.240	9.16E-6
	0.240	3.61E-6	0.315	3.32E-9	0.220	6.09E-6
	0.220	2.25E-6	0.312	2.96E-9	0.200	3.53E-6
	0.200	1.34E-6	0.262	3.84E-10	0.180	1.65E-6
	0.180	7.56E-7	0.212	3.49E-10	0.160	5.01E-7
	0.160	4.00E-7	0.162	1.79E-12	0.140	3.62E-8
	0.140	1.95E-7	0.112	3.28E-14	0.135	6.65E-9
	0.120	8.54E-8			0.132	6.45E-10
	0.100	3.22E-8			0.1308	4.73E-11
	0.080	9.83E-9			0.1305	9.10E-12
	0.060	2.14E-9				
	0.040	2.50E-10				
	0.020	6.44E-12				
	0.010	1.67E-13				
FIT PARAMETER Ks	4.4E-3		2.00E-4		2.00E-4	

Appendix B

Runge-Kutta Method for Calculating Water Content

1.0 Purpose

This Appendix describes the development and testing of a numerical method implemented in the GoldSim DU PA model for estimating the volumetric water content of the waste, clay liner and native Unit 3 soil below the Federal DU cell at the Energy*Solutions* Clive Facility.

2.0 Method

The flow of water in porous media occurs in response to a gradient in the total potential energy of water. The total potential can be composed of a number of components but this analysis will be restricted to gravitational and matric potentials. Water potential components are often expressed in units of energy per unit weight rather than units of energy per unit mass. When the quantity of water is expressed as a weight, the units of potential are defined in terms of head. The gravitational potential refers to the energy of water with respect to reference elevation and is written here as Z. Although not a formal definition, the matric potential relates to the energy of the tension imposed on the pore water by the soil matrix. Matric potential is a negative value and is written here as ψ. The total potential is then H = ψ + Z.

Steady-state fluid flow in an unsaturated medium is defined by the Buckingham-Darcy equation (Jury and Horton, 2004, p.95). In the following discussion this equation will be referred to simply as the Darcy equation. The one dimensional form of Darcy's equation for unsaturated flow is given by Fayer (2000, Eqns. 4.2 and 4.5):

$$q = -K_L(\psi)\frac{\partial H}{\partial z} \tag{1}$$

where

q	is the flux of liquid per unit area,
K_L	is the unsaturated conductivity as a function of the matric potential ψ,
H	is the matric plus gravitational potentials [cm], and
z	is the depth below ground surface [cm].

It is convenient to define two sign conventions for the total potential (Fayer 2000, page 4.2): (1) the *z*-coordinate is zero at the soil surface and positive downward. With this convention, the gravitational head in the soil, which is defined as the elevation of a point with respect to the soil surface, and negative and defined as -*z*; and (2) the suction head, *h*, is the negative of the matric potential or matric head, ψ. With this convention, the suction head, *h*, is always greater than zero for an unsaturated soil. It follows that

$$H = \psi + Z = -(h + z) \tag{2}$$

and the flux is then given by

$$q = K_L(h)\left[\frac{\partial h}{\partial z} + 1\right] \tag{3}$$

The unsaturated conductivity, K_L, is formulated based on the Brooks-Corey representation for moisture content as a function of suction head

$$\begin{aligned} \Theta &= \frac{h}{h_b}^{-\lambda} \quad \text{for} \quad h > h_b, \\ &= 1 \quad \text{for} \quad 0 \le h \le h_b \end{aligned} \tag{4}$$

where

Θ is the effective saturation,

h is the suction head (cm),

h_b is the bubbling pressure head (cm) at which moisture first drains from the material, and

l is a constant that is fit to data.

Alternatively, expressed in terms of the fractal dimension, D

$$\begin{aligned} \Theta &= \frac{h}{h_b}^{D-3} \quad \text{for} \quad h > h_b, \\ &= 1 \quad \text{for} \quad 0 \le h \le h_b \end{aligned} \tag{5}$$

The suction head is positive for an unsaturated material and 0 at saturation. θ_s, the effective saturation, is defined as

$$\Theta = \frac{\theta - \theta_r}{\theta_s - \theta_r}, \tag{6}$$

where

Θ is the moisture content,

Θ_r is the residual moisture content, and

Θ_s is the saturated moisture content.

Combining Equations

$$\theta = \theta_r + \theta_s - \theta_r \frac{h}{h_b}^{-\lambda} \tag{7}$$

This equation can then be fit to core data.

Alternatively, expressing in terms of D and assuming

$$\theta = \theta_r + (\theta_s - \theta_r) \frac{h}{h_b}^{(D-3)} \tag{8}$$

Using the Mualem theory for predicting hydraulic conductivity (Mualem 1976), the unsaturated

hydraulic conductivity is defined as

$$K_L = K_S \Theta^{2+\frac{2}{\lambda}}. \tag{9}$$

Substituting Equation 6 into Equation 9 gives:

$$K_L = K_S \frac{\theta - \theta_r}{\theta_s - \theta_r}^{2+\frac{2}{\lambda}}. \tag{10}$$

The computational method implemented in the Clive DU PA Model solves Equation 3 for steady state flow at constant infiltration flux, q. (At steady state, the vertical infiltration flux must be constant in all layers of the cell below the radon barriers, which includes the waste, the clay liner, and the unsaturated zone.) No iterations are required with the selected solution technique. The approach in the Clive DU PA Model differs from the solution technique in the UNSAT-H code, which solves the transient (unsteady) equation for one-dimensional unsaturated flow and iterates to a steady state solution with constant infiltration rate.

3.0 Solution of the Darcy Equation by the Runge-Kutta Method

Equation 3 is a nonlinear, first order differential equation for the suction head that can be solved by numerical approximation. The Runge-Kutta method is attractive for this application because it allows variable spacing (i.e., variable Δz) between nodes, because it is highly stable, and because it does not require iteration to converge to a solution. Equation 3 can be rewritten as a first order differential equation in the form $h' = f(h)$:

$$\frac{\partial h}{\partial z} = \frac{q}{K_L(h)} - 1 \tag{11}$$

A second order Runge-Kutta solution for this first order differential equation is given by Abramowitz and Stegun (1970, Section 25.5.6):

$$h_{n+1} = h_n + \frac{k_1 + k_2}{2} + O(h^3), \tag{12}$$

with

$$k_1 = \Delta z \frac{q}{K_L(h_n)} - 1 \tag{13}$$

$$k_2 = \Delta z \left(\frac{q}{K_L(h_n + k_1)} - 1 \right) \tag{14}$$

and

$$\Delta z = z_{n+1} - z_{n.} \quad (15)$$

Equations 12 through 15 define a procedure for calculating h_{n+1} from the known values of h_n, Δz, and the (constant) infiltration flux, q. These equations constitute a predictor-corrector calculation, where k_1 is the predictor and k_2 is the corrector. No iteration is involved in this solution because Equations 13, 14, and 12 can be solved sequentially for each node of the grid, beginning with the lowest node at the top of the water table with $h = 0$ (because the suction head is zero for a saturated soil) and $K_L = K_s$, and integrating upward through the various unsaturated soil layers. Stable solutions do require a finer discretization than the layers that are defined for the 1-D columns used in the Clive PA model.

The value of Δz does not have to be constant over the domain of integration, and has been adjusted to provide reasonable accuracy where the head gradient is greatest. In practice, these regions occur at the capillary fringe just above the water table and at the interface between the clay liner and waste. The value of Δz has to be small enough that the predictor step (Equation 13) does not generate a value of k_1 that is so large and negative that $(h_n + k_1)$ becomes negative. Suction head is always positive, and $K_L(h_n + k_1)$ in Equation 14 cannot be evaluated for negative values of $(h_n + k_1)$. In practice, an initial node spacing of 2 cm provides a stable solution in Unit 3, directly above the water table, for the infiltration fluxes of interest. However, an initial node spacing of 0.1 mm was required to provide a stable solution in the waste, directly above the clay liner, at high infiltration rates. This fine spacing is required because the head gradient at the interface between the waste and clay liner is quite large. A node spacing of 25 cm provides a stable solution in the main body of the waste and in Unit 3 where the head gradients are smaller. A constant node spacing of 15 cm provides adequate resolution in the clay liner and in the upper and lower radon barrier. Solutions at these variable grid spacings are mapped to the Clive DU PA Model's regular grid that is used to represent wastes and other layers, in the top slope and side slope columns.

4.0 Verification of the Runge-Kutta Method

The UNSAT-H modeling program (Fayer 2000) has been used to analyze infiltration through the Federal DU cell at the EnergySolutions facility (Whetstone 2007). A model built with UNSAT-H predicted moisture content and suction head from the radon barriers in the cover downward through the waste, clay liner, and Unit 3 silty sand to the top of the aquifer (Whetstone 2007, Section 4 and Table 17). The results from the UNSAT-H calculation for the top and side slope models have been used to verify the steady state unsaturated flow solutions with the Runge-Kutta method outlined in Section 3.

The UNSAT-H calculations are based on a van Genuchten representation for soil moisture content and for soil hydraulic conductivity. For verification purposes, the Runge-Kutta solution was programmed into a spreadsheet using the identical van Genuchten models as UNSAT-H. The Runge-Kutta verification used the same total thicknesses for the radon barriers, waste, clay liner, and Unit 3 sand as the UNSAT-H model, but the spacing of individual nodes (i.e., the values of Δz) is different. Table 1 summarizes the thicknesses of the major components.

Table 1. Layer thicknesses and coordinates for top slope validation calculations.

Layer	Thickness	z-Coordinate
Upper Radon Barrier	1 ft (30.48 cm)	0 to 30.48 cm
Lower Radon Barrier	1 ft (30.45 cm)	30.48 cm to 60.96 cm
Waste	45 ft (1371.6 cm)	60.96 cm to 1432.56 cm
Clay Liner	2 ft (60.96 cm)	1432.56 cm to 1493.52 cm
Unit 3 Silty Sand	10.8 ft (329.2 cm)	1493.52 cm to 1822.7 cm

Figure 1(a) compares the calculated values for moisture content from the UNSAT-H model (Whetstone 2007, Table 17) and from the Runge-Kutta solution for the top slope model with an infiltration rate of 0.276 cm/yr. Both solutions encompass the radon barriers, the waste, the clay liner beneath the waste, and Unit 3 from the bottom of the clay liner to the top of the water table. The results are essentially identical, providing validation for the Runge-Kutta method. Figure 1(b) provides a more detailed comparison of moisture content near the bottom and top of the clay liner, again demonstrating the close agreement between the UNSAT-H model and the Runge-Kutta method.

A similar comparison was also performed for the side slope model with an infiltration rate of 0.595 cm/yr. The side slope model is similar to the top slope model, except the average waste thickness is 5.64 m (18.5 ft) rather than 13.7 m (45 ft). Figures 2(a) and 2(b) again demonstrate the close agreement between the UNSAT-H model and the Runge-Kutta method.

The calculated values for suction head from the UNSAT-H model and from the Runge Kutta method were also compared for the top and side slope models. The suction head profiles in the radon barriers, waste, clay liner and Unit 3 are shown in Figure 3 for the top and side slope models. A qualitative comparison between the Runge-Kutta solution and the UNSAT-H results was performed because the UNSAT-H data for suction head were not tabulated, only presented graphically (Whetstone 2007, Figures 8 and 9). The comparison of suction heads from both methods again demonstrates that the Runge-Kutta solution is in excellent agreement with the results from the UNSAT-H model.

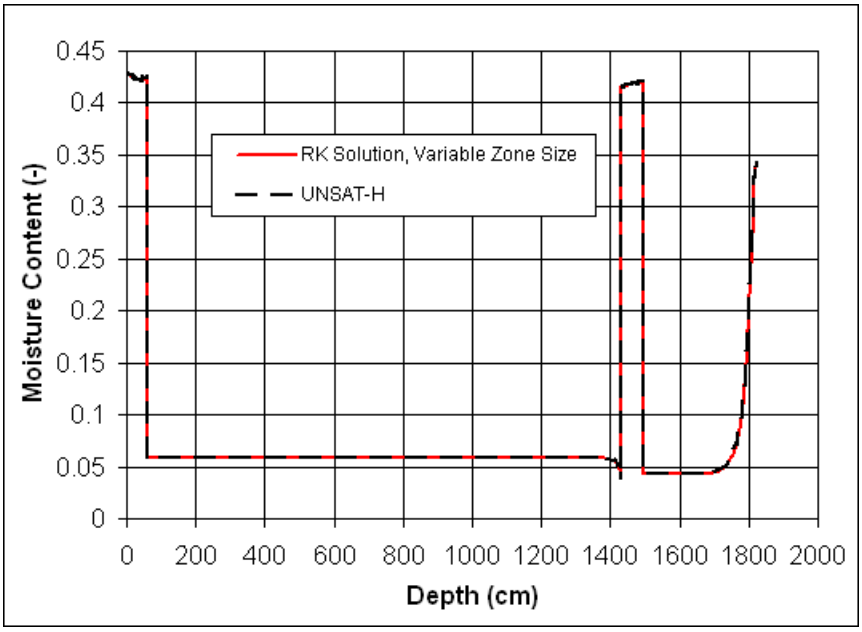

a) Comparison of moisture content in Unit 3, clay liner, waste, and radon barriers

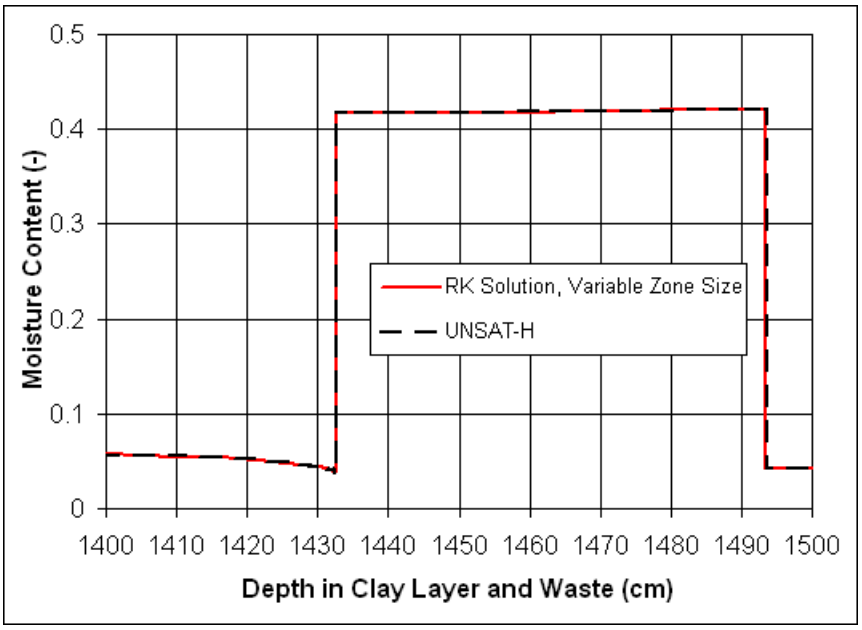

b) Comparison of moisture content in and adjacent to the clay liner

Figure 1. Comparison of the Runge-Kutta and UNSAT-H solutions for top slope model.

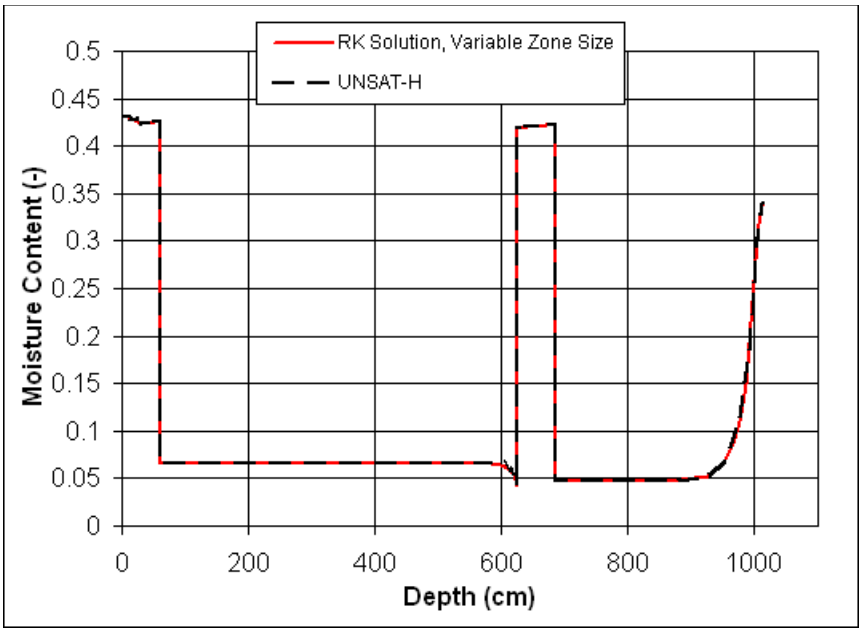

(a) Comparison of moisture content in Unit 3, clay liner, waste, and radon barrier

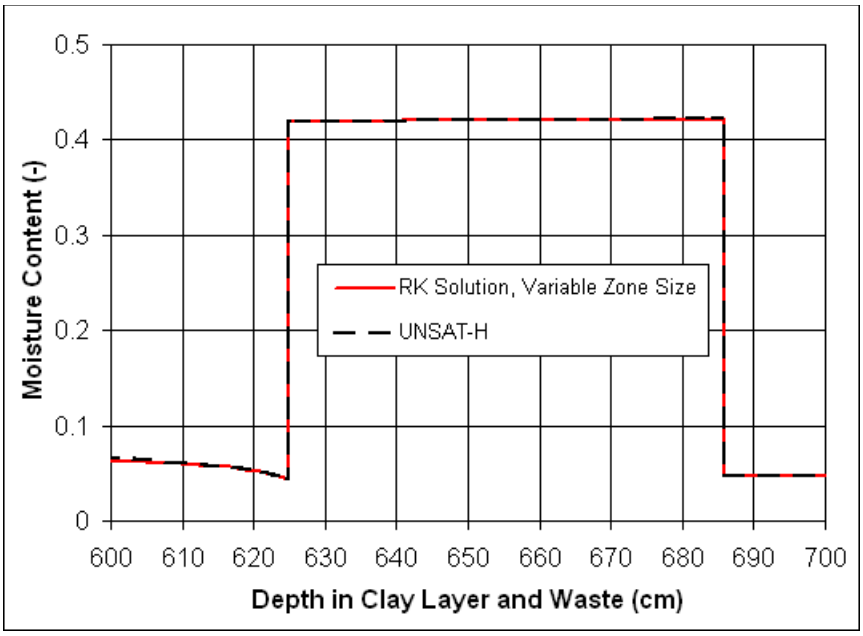

(b) Comparison of moisture content in and adjacent to the clay liner

Figure 2. Comparison of the Runge-Kutta and UNSAT-H solutions for side slope model.

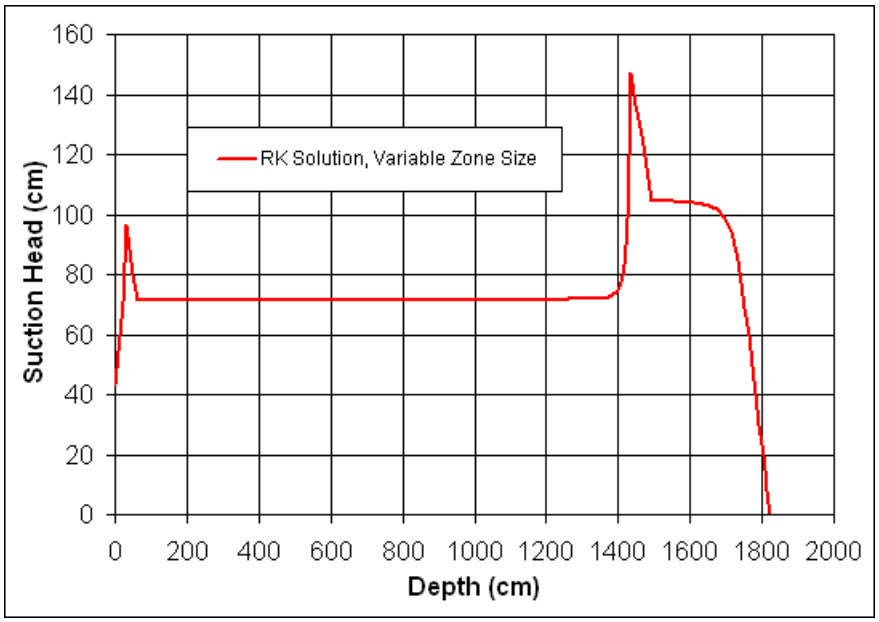

(a) Top Slope Model

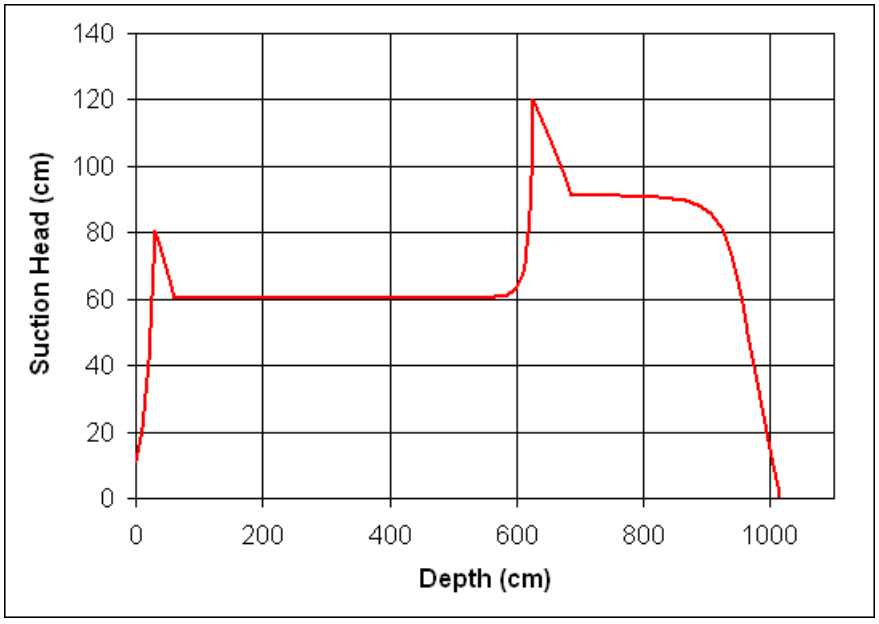

b) Side Slope Model

Figure 3. Suction head profiles in Unit 3, clay liner, waste, and radon barriers for the top slope and side slope models.

The results in Figures 1 and 2 highlight three important features of the response of the Federal DU cell to infiltration. First, the clay liner has a moisture content of about 0.42 (see Figures 1(b) and 2(b)) in the top and side slope models. This value is just below θ_s, which is 0.432 for the van Genuchten model. The radon barriers have slightly higher moisture contents, approximately

0.425 to 0.43 (see left-hand side of Figures 1(a) and 2(a)), again just below the saturated moisture content of 0.432. These results confirm that the clay liner and radon barriers remain very close to saturation for either model (top or side slope) and for two different infiltration rates (0.276 cm/yr or 0.595 cm/yr) in the Federal DU cell. Second, the waste drains to a relatively low moisture content, on the order of 0.06 for either slope model and infiltration rate. This behavior is consistent with the low moisture retention of a sandy material. Finally, suction head shows greater differences than moisture content for the top and side slope models. The suction head is more directly dependent on flow rate (see Equation 11) than moisture content, and the factor of two difference in the flow rates for the top and side slope models is the probable cause of the differences in Figure 3(a) and 3(b).

5.0 Implementation in the DU PA Model

The Runge-Kutta method has been incorporated into the Clive PA model for infiltration through the radon barriers, waste, clay liner and Unit 3 of the Federal DU cell at the EnergySolutions facility. The PA model of the Federal DU cell has a number of differences with the verification calculations discussed in the previous section. The major differences are as follows:

1. The moisture retention and hydraulic conductivity of the radon barriers and clay liner are defined by a Brooks-Corey/Mualem model that is based on the test data from Colorado State University (Bingham Environmental 1991, Appendix B, pages B-20 and B-26) for Unit 4 cores GW17A B2 and GW19A B1.
2. The moisture retention and hydraulic conductivity of the Unit 3 silty sand between the clay liner and water table are defined by a Brooks-Corey/Mualem model that is based on the test data from Colorado State University (Bingham Environmental 1991, Appendix B, pages B-20 and B-26) for Unit 3 cores GW18 B4 and GW17A B5.

Integration of the Darcy equation from node n, with a known value of the suction head, h_n, and a known value of $\Delta z_n = z_{i+1} - z_n$, to node n+1 is based on the following sequential steps:

1. Calculate the moisture content, θ_n, corresponding to the suction head, h_n. The calculation of θ_n, is based on Equations 4 and 6 in Section 2.
2. Calculate the conductivity, $K(h_n)$, based on the effective saturation, Θ_n, at θ_n. Equations 6 and 9 in Section 2 define the formulas.
3. Calculate $k_1 = \Delta z_n(q/K(h_n) - 1)$ (see Equations 13 and 15 in Section 3).
4. Calculate the trial value of the suction head, $h_n + k_1$.
5. Calculate the trial value of the moisture content, $\theta\,(h_n + k_1)$ using Equations 4 and 6 found in Section 2.
6. Calculate the trial value of the conductivity, $K(h_n + k_1)$, based on the effective saturation at $\theta\,(h_n + k_1)$. Equations 6 and 9 in Section 2 define the formulas.
7. Calculate $k_2 = \Delta z_n(q/K(h_n + k_1) - 1)$ (see Equations 14 and 15 in Section 3).
8. Calculate $h_n + 1 = h_n + (k_1 + k_2)/2$ (see Equation 12 in Section 3).

Numerical testing demonstrated that the trial value of the suction head, $h_n + k_1$, can become

negative, leading to an undefined value for $K(h_n + k_1)$. Negative values of $K(h_n + k_1)$occurred at the interface between the waste and clay liner when the infiltration rate increased from 0.3 to 0.5 cm/yr for the as-designed cover to approximately 5 cm/yr. The numerical problem appears in the waste, adjacent to its interface with the clay liner, because the gradient of suction head is greatest at this location (for example, see Figure 3(a) at a depth of about 1,400 cm).

The verification testing in Section 3 used the following spacing for nodes in the waste, adjacent to the clay liner: (1) 2 cm node spacing for the first five nodes in the waste, (2) 5 cm node spacing for the next 4 nodes in the waste, and (3) 25 cm node spacing for all other nodes in the waste. The GoldSim implementation of this solution uses a geometric spacing between the first 12 nodes in the waste, beginning with an initial spacing of 0.1 mm, which increases by a ratio of approximately 1.93 for each subsequent node. The spacing between the 11th and 12th nodes is 0.135 m and the total width of the 12 nodes with geometric zoning is 0.281 m. All subsequent nodes in the waste have a constant spacing of 0.281 m in the GoldSim implementation. Numerical testing demonstrated that the geometric zoning produces stable solutions for the top slope and side slope models with the Runge-Kutta method up to flow rates of 5 cm/year.

6.0 Numerical Testing of the Top Slope Model in GoldSim

Validation of a top slope infiltration model for the Federal DU cell was performed in GoldSim, using the same Runge-Kutta method and the same descriptions of soil properties, providing a direct comparison of results and a means of identifying errors in programming. Deterministic calculations were performed with Brooks-Corey/Mualem models for the individual cores (Unit 4 core GW17A B2 or GW19A B1, and Unit 3 core GW17A B5 or GW18 B4) to compare unsaturated flow conditions calculated using GoldSim. Stochastic calculations were performed with GoldSim for 20 realizations using randomly sampled values for the Brooks-Corey/Mualem input parameters for Units 3 and 4. The GoldSim results for Realization 18 were identical to a calculation for Realization 18 to 5 or 6 significant digits. This testing also provided useful insights into the range of conditions in the Federal DU cell during unsaturated flow.

Figures 4 and 5 compare the profiles for moisture content and suction head, respectively, in the radon barriers, waste, clay liner, and Unit 3 for the four deterministic calculations that use Unit 3 (silty sand) properties for GW18 B4 or GW17A B5 and use Unit 4 (silty clay) properties for GW17A B2 or GW19A B1. All calculations have an infiltration rate of 0.276 cm/yr (0.109 in/yr). These results confirm previous observations: (1) The moisture contents of the clay liner and radon barriers remain close to saturation, and (2) the waste retains a low moisture content of 0.06. In addition, the suction heads in the radon barriers are identical because the hydraulic conductivity is identical for either core (because conductivity was only measured for one of the two cores).

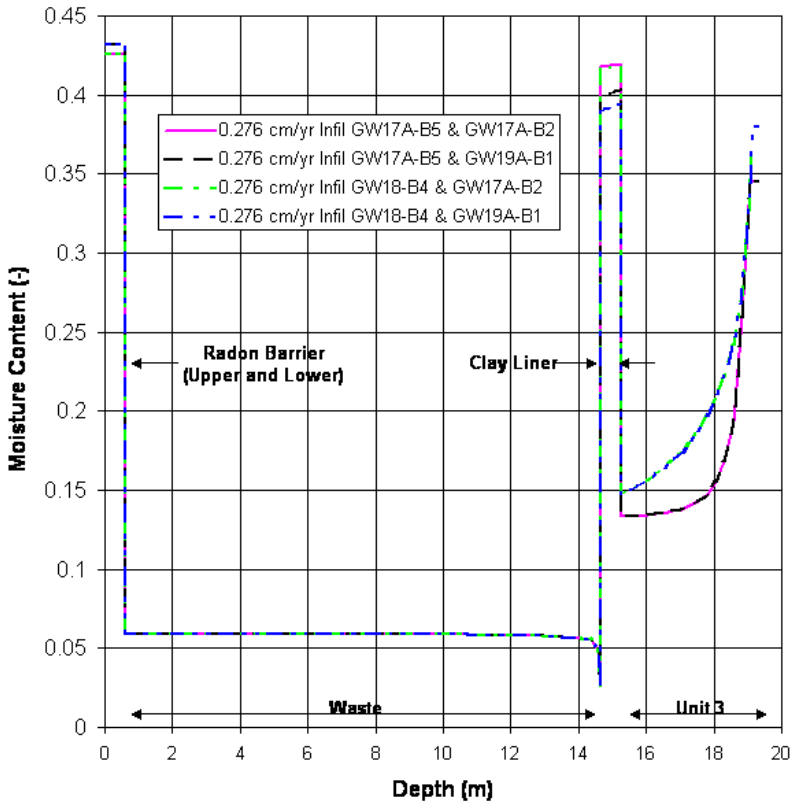

Figure 4. Profiles of moisture content in Unit 3, clay liner, waste, and radon barriers for the top slope model with 0.276 cm/yr infiltration.

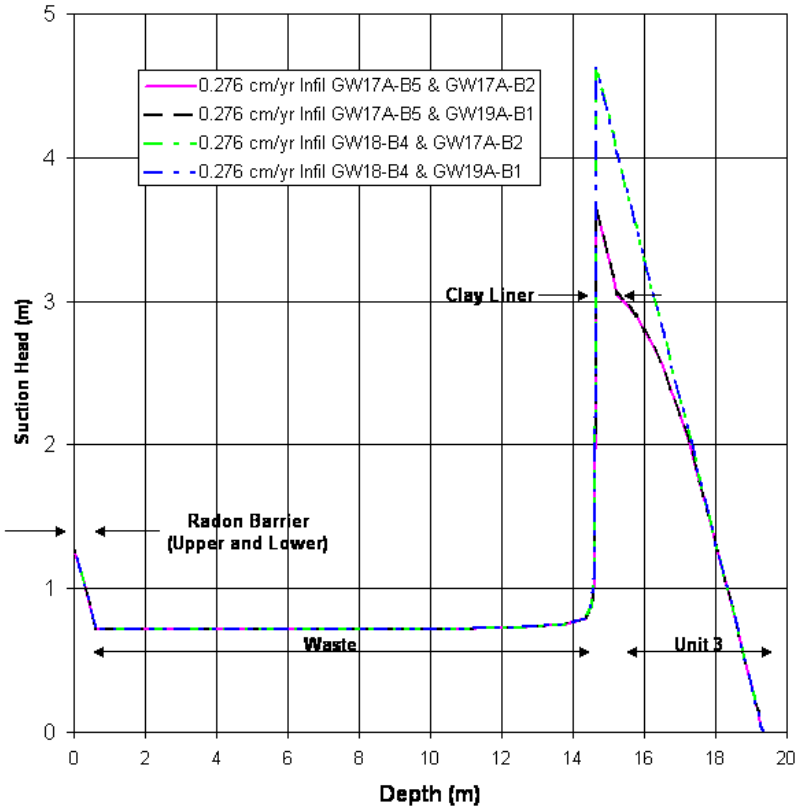

Figure 5. Profiles of suction head in Unit 3, clay liner, waste, and radon barriers for the top slope model with 0.276 cm/yr infiltration.

Figures 6 and 7 compare the profiles for moisture content and suction head, respectively, in the radon barriers, waste, clay liner, and Unit 3 for deterministic calculations that use soil properties for GW17A-B5 (Unit 3) and GW17A-B2 (Unit 4) at three different infiltration rates: 0.168 cm/year, 0.276 cm/yr, and 5.0 cm/yr. In general, Figures 8 and 9 demonstrate that moisture content is more sensitive to infiltration rate than to the differences between soil properties for the various cores. The major difference in Figure 6 is the degree of drainage in the waste, with the high infiltration rate increasing the retained moisture from 0.055 at 0.168 cm/yr to 0.084 at 5.0 cm/yr infiltration. The moisture content in the waste also shows a small oscillation between 0.082 to 0.086 at the 5.0 cm/yr infiltration rate. This could have be eliminated by having finer spacing between the nodes in the waste, but the accuracy of the current solution is considered more than adequate. Similar calculations were also performed for soil properties with GW17A-B5 for Unit 3 and GW19A-B1 for Unit 4. The results are very similar to those shown in Figures 6 and 7 and are not repeated here.

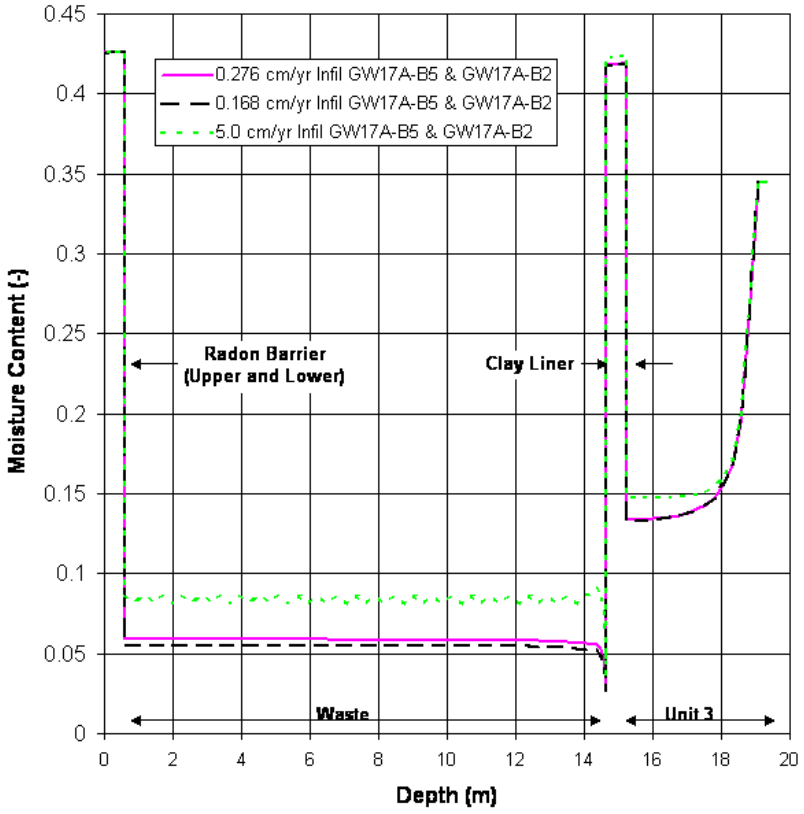

Figure 6. Profiles of moisture content in Unit 3, clay liner, waste, and radon barriers for the top slope model with different infiltration rates.

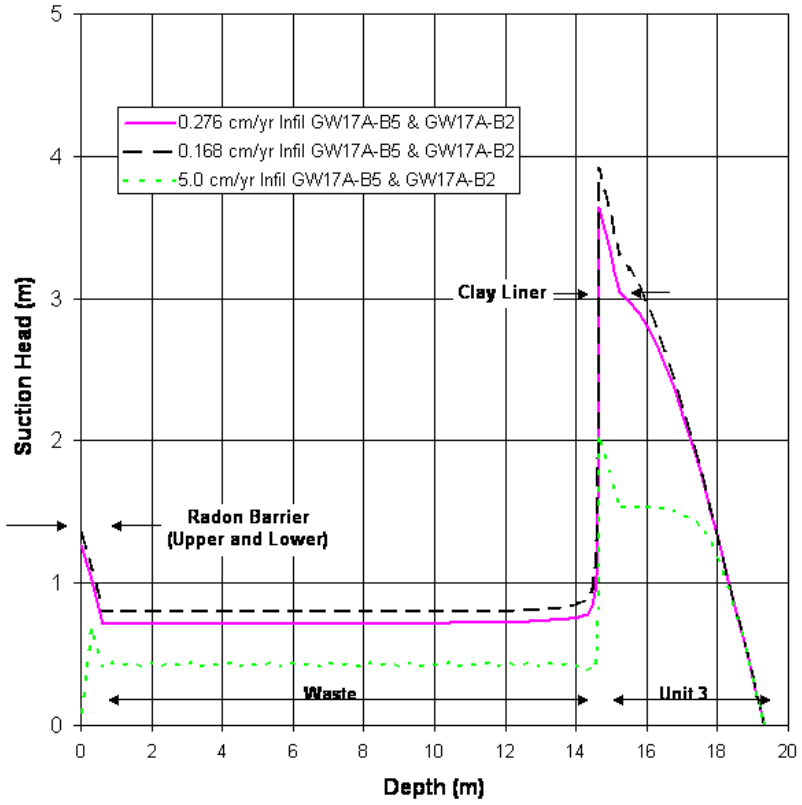

Figure 7. Profiles of suction head in Unit 3, clay liner, waste, and radon barriers for the top slope model with different infiltration rates.

Figures 8 through 12 compare the time dependent moisture content at the mid-points of Unit 3, of the clay liner, of the waste, of the lower radon barrier, and of the upper radon barrier, respectively, for a GoldSim calculation with 20 realizations and randomly sampled soil properties for Units 3 and 4. The duration of each realization is 3,000 years and the lower filter layer is assumed to become degraded at 2,640 years after closure for test purposes.

The results in Figures 8 through 12 confirm the observations from the previous calculations: (1) the moisture contents in the clay liner, lower radon barrier, and upper radon barrier remain close to saturation (note the expanded vertical scale for Figures 11 and 12), and (2) the waste drains to low moisture content, 0.03 to 0.08, for these 20 realizations, and (3) the moisture content in Unit 3 also has a limited range of 0.13 to 0.20 for the infiltration rates generated by the cover infiltration model.

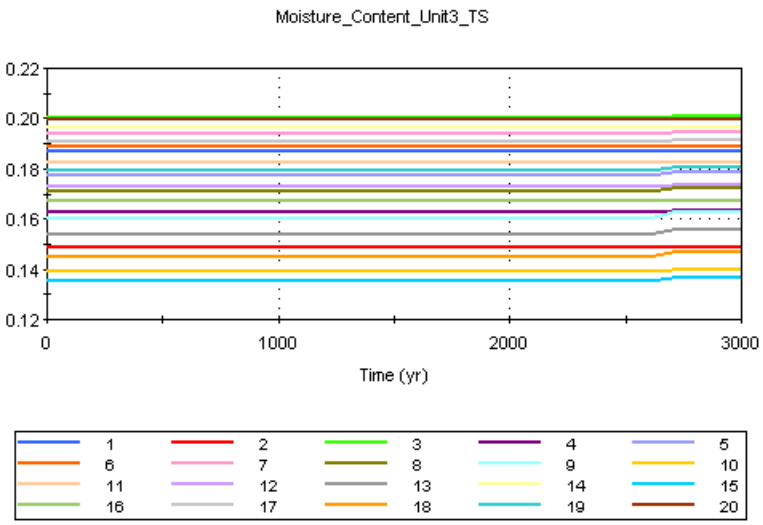

Figure 8. Time dependent moisture content from 20 realizations at the mid-height of Unit 3 with sampled soil properties for Units 3 and Unit 4.

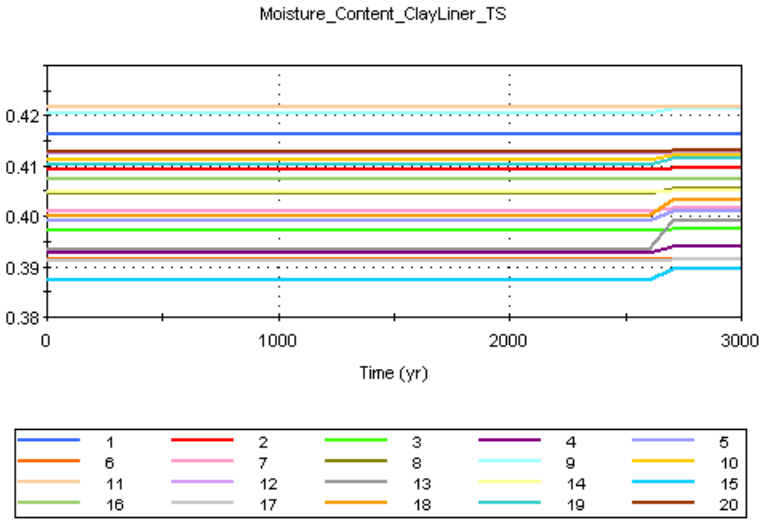

Figure 9. Time dependent moisture content from 20 realizations at the mid-height of the clay liner with sampled soil properties for Units 3 and Unit 4.

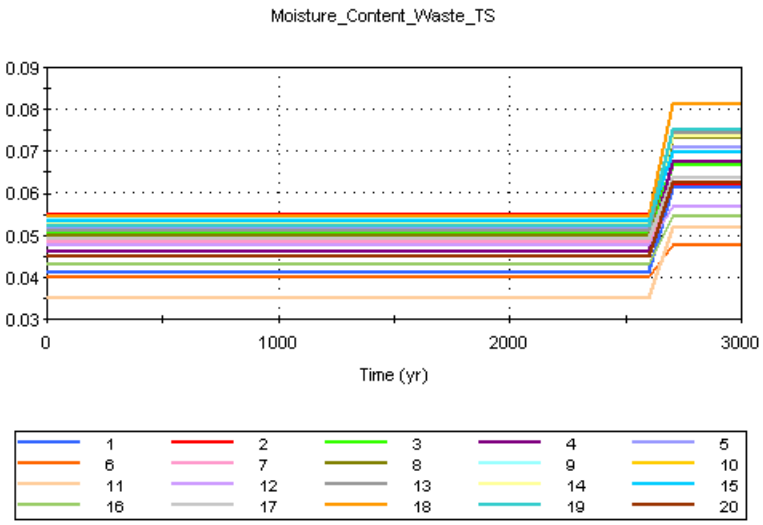

Figure 10. Time dependent moisture content from 20 realizations at the mid-height of the waste with sampled soil properties for Units 3 and Unit 4.

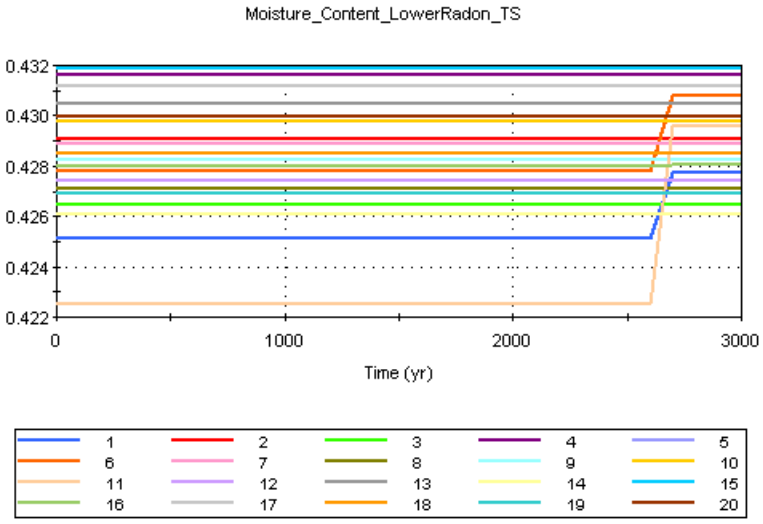

Figure 11. Time dependent moisture content from 20 realizations at the mid-height of the lower radon barrier with sampled soil properties for Units 3 and Unit 4.

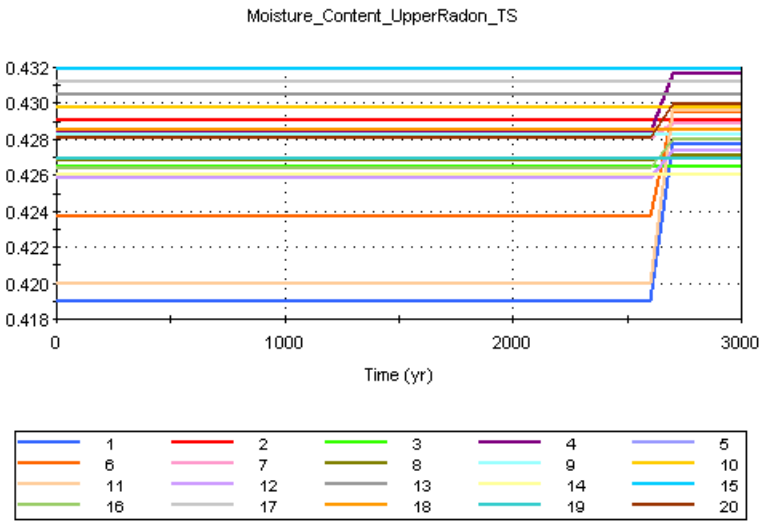

Figure 12. Time dependent moisture content from 20 realizations at the mid-height of the upper radon barrier with sampled soil properties for Units 3 and Unit 4.

8.0 References

Abramowitz, Milton, and Irene A. Stegun, 1970. *Handbook of Mathematical Functions with Formulas, Graphs, and Mathematical Tables*. National Bureau of Standards, Applied Mathematics Series 55, ninth printing. November, 1970.

Bingham Environmental, 1991. *Hydrogeologic Report Envirocare Waste Disposal Facility South Clive, Utah*. Final version October 9, 1991.

Fayer, M.J., 2000. *UNSAT-H Version 3.0: Unsaturated Soil Water and Heat Flow Model, Theory, User Manual, and Examples*. PNNL-13249. Pacific Northwest National Laboratory, Richland, Washington. June, 2000.

Jury, W.A. and R. Horton. 2004. *Soil Physics*. 6th ed. John Wiley and Sons Inc. New Jersey.

Mualem, Yechezkel, 1976. *A New Model for Predicting the Hydraulic Conductivity of Unsaturated Porous Media*. Water Resources Research, Vol. 12, No. 3, pp. 513-522. June, 1976.

Whetstone Associates, Inc., 2007. *EnergySolutions Class A South Cell Infiltration and Transport Modeling*. December 7, 2007.